Radiation Fibrosis of the Vocal Fold: From Man to Mouse

Michael M. Johns, M.D[1], **Vasantha Kolachala, Ph.D.**[2], **Eric Berg, M.D.**[3], **Susan Muller, D.M.D**[4], **Frances X. Creighton, B.S.**[2], and **Ryan C. Branski, Ph.D.**[5]

[1]Associate Professor, Otolaryngology – Head and Neck Surgery. Director, Emory Voice Center. Emory University. Atlanta, GA

[2]Research Associate, Otolaryngology – Head and Neck Surgery. Emory University. Atlanta, GA

[3]Resident Physician, Otolaryngology – Head and Neck Surgery. Emory University. Atlanta, GA

[4]Professor, Otolaryngology – Head and Neck Surgery and Pathology, Emory University. Atlanta, GA

[5]Associate Professor, Otolaryngology – Head and Neck Surgery. Associate Director, NYU Voice Center. New York University. New York, NY

Abstract

Objectives—To characterize fundamental late tissue effects in the human vocal fold following radiation therapy. To develop a murine model of radiation fibrosis to ultimately develop both treatment and prevention paradigms.

Design—Translational study using archived human and fresh murine irradiated vocal fold tissue.

Methods—**1**) Irradiated vocal fold tissue from patients undergoing laryngectomy for loss of function from radiation fibrosis were identified from pathology archives. Histomorphometry, immunohistochemistry, and whole-genome microarray as well as real-time transcriptional analyses was performed. **2**) Focused radiation to the head and neck was delivered to mice in a survival fashion. One month following radiation, vocal fold tissue was analyzed with histomorphometry, immunohistochemistry, and real-time PCR transcriptional analysis for selected markers of fibrosis.

Results—Human irradiated vocal folds demonstrated increased collagen transcription with increased deposition and disorganization of collagen in both the thyroarytenoid muscle and the superficial lamina propria. Fibronectin were increased in the superficial lamina propria. Laminin decreased in the thyroarytenoid muscle. Whole genome microarray analysis demonstrated increased transcription of markers for fibrosis, oxidative stress, inflammation, glycosaminoglycan production and apoptosis. Irradiated murine vocal folds demonstrated increases in collagen and fibronectin transcription and deposition in the lamina propria. Transforming growth factor (TGF)-β increased in the lamina propria.

Conclusion—Human irradiated vocal folds demonstrate molecular changes leading to fibrosis that underlie loss of vocal fold pliability that occurs in patients following laryngeal irradiation.

Irradiated murine tissue demonstrates similar findings, and this mouse model may have utility in creating prevention and treatment strategies for vocal fold radiation fibrosis.

Keywords

vocal fold; larynx; dysphonia; radiation; fibrosis

INTRODUCTION

The larynx is one of the most common primary sites of squamous cell carcinoma in the head and neck. In an effort to preserve the larynx and its function, radiation with or without concurrent chemotherapy is the preferred treatment for most patients with laryngeal squamous cell carcinoma. Although effective, radiation to the vocal folds is associated with significant functional limitations.[1] Radiation therapy to the larynx specifically results in damage to the vocal folds and surrounding tissue, with a fibroblastic response hypothesized to be related to acute oxidative injury with resulting cell damage, ischemia, and inflammatory response.[2]

Radiation changes to tissue occur along a continuum but can be aggregated into acute and chronic changes. Acutely, radiation leads to injury and death of dividing cells. This is the therapeutic principle upon which radiation is based due to the rapid cellular growth of neoplastic tissue. However, radiation acutely leads to injury of normal tissue as well. Common early effects include mucosal edema, necrosis, and sloughing. Rapidly dividing salivary gland tissue is damaged. Muscular edema and injury can contribute to acute dysfunction as well. Over months following radiation, the acute inflammatory changes resolve and collagen deposition occurs resulting in tissue fibrosis.[2] In the larynx, the loss of vocal fold pliability chronically related to radiation fibrosis is thought to lead to hoarseness, inability to be heard over noise, and vocal strain with communication. These symptoms impair patients' quality of life after treatment. Although this morbidity has been described extensively following radiation to the vocal folds for glottal tumors, recent research has confirmed decreased phonatory function following radiation for non-glottal tumors as well. A recent study comparing vocal parameters in patients receiving radiation therapy for glottal versus non-glottal tumors suggests that wide-field radiation may in fact have a more significant impact on voice than localized radiation for glottal malignancy alone.[3]

Current therapy for this condition is largely supportive without any effective interventions to date, contributing to the significant need for research regarding improved treatment strategies for these challenging patients. Investigation regarding laryngeal fibrosis due to other etiologies provides a number of possible interventions, including a variety of injections such as mesenchymal stem cells and growth factor therapy.[4,5] Although such interventions have been investigated in existing mouse models, no well-defined model for radiation has been developed.[5] This paucity of literature is significant in that even though fibrotic changes are evident in the aged and injured larynx, the pathophysiologic process of radiation-induced fibrosis is likely unique and therefore interventions that may prove efficacious for age-induced or traumatic fibrosis cannot be presumed effective for radiation fibrosis. Therefore, in order to further investigate potential therapeutic interventions to reverse or prevent the fibrotic tissue changes associated with external beam therapy to the larynx, elucidation of fundamental changes occurring in irradiated vocal fold tissue at the transcriptional and translational levels is needed. In fact, there have been no published reports comparing radiated to non-radiated human vocal fold tissue in a controlled fashion. With an improved understanding of critical biochemical changes following radiation, potential targets for intervention can be developed to prevent and/or treat radiation-induced vocal fold fibrosis.

The development of an animal model to test these interventions is another crucial step towards treating radiation fibrosis of the vocal fold in humans.

The first aim of this study was to characterize basic biochemical events in the human vocal fold following radiation. This aim involved the analysis of archived human tissue from previously banked by the Department of Pathology at a tertiary academic medical center. Specimens from patients who received radiation therapy for laryngeal squamous cell carcinoma without evidence of persistent or recurrent disease were evaluated. Histomorphometry and immunohistochemistry are used to characterize translational changes in the structure and extracellular matrix composition of the vocal fold, compared to non-radiated vocal fold tissue. In addition, whole-genome microarray analysis and real-time PCR assessment of irradiated versus non-irradiated vocal fold tissue was performed.

The second aim of this study is to develop a murine model of radiation-induced laryngeal fibrosis developed from an existing model of radiation-induced pulmonary fibrosis.[6] This existing model has been productive in the investigation of fibrotic change in the lung, and similar productivity can be expected of models of radiation-induced changes elsewhere. The use of a murine model for radiation-induced laryngeal fibrosis is an attractive option due to its size, affordability, and wide variety of available genetic strains and reagents. It should be noted that mice do not share the identical microanatomical architecture of the vocal fold as humans with epithelium overlying superficial, intermediate and deep lamina propria covering thyroarytenoid muscle. However, they do have a vocal fold distinct lamina propria that shares histomorphometric properties with humans and shows changes similar to humans in other pathologic models.[7] The development a murine model for radiation fibrosis can allow for further characterization of the fibrotic process induced by radiation itself in the larynx. Perhaps more importantly, this model provides for detailed investigation regarding a variety of potentially therapeutic modalities, including the injection of immediate and controlled-release preparations of growth factors, pharmacologic agents, stem cells, and other biologic agents, in the treatment of radiation-induced laryngeal fibrosis.

Although, the development of improved treatment strategies for radiation fibrosis is needed, improved knowledge of the impact of radiation on vocal fold tissue at a molecular and cellular level is a prerequisite for appropriate investigation.

METHODS

Human Vocal Fold Studies

Tissue Selection—With approval from the Institutional Review Board, archived vocal fold specimens from patients between 1990 and 2008 were obtained from a tertiary academic medical center. All specimens were from patients undergoing post-radiation salvage laryngectomies, with a history of head and neck cancer. Specimens with reported evidence of persistent or recurrent disease at the time of surgical excision were excluded. Tissue blocks were pulled from storage and grossly assessed for adequate tissue quality. The medical records of the patients associated with suitable specimens were then evaluated and cross-referenced with pathologic data in order to confirm the clinical history of radiation treatment prior to surgical management. Demographic patient data including patient sex and age at time of surgery were noted. The site of the primary tumor, reason for laryngectomy, timing of surgical excision in relation to radiation treatment, specifics of radiation treatment, and history of adjunctive chemotherapeutic management were noted when available.

To ensure that observed tissue changes were due to radiation and not treatment for the malignant disease process, tissue from the within the field of radiation was included and tissue from the primary sub site was excluded. Specifically, if the initial tumor was

supraglottal or subglottal alone and not involving the glottis, both vocal folds were included for evaluation. If the initial tumor was glottal in origin, only the contralateral, uninvolved fold was evaluated. In order to avoid skewing data during statistical analyses, only one vocal fold per patient was included, even when both cords met inclusion criteria.

Once suitable specimens were identified and collected, control samples were also collected from three adult human male autopsy specimens with no history of intubation, laryngeal carcinoma, or radiation treatment. The specific markers of vocal fold fibrosis were chosen based on previously observed changes in animal vocal fold models, as well as in radiation-induced pulmonary and renal fibrosis.[6, 8–11]

Histomorphometry and Immunohistochemistry

General tissue methodology: All gross observations of tissue architecture and quantifiable measurements related to histology were completed in a blinded manner for both radiated tissue and controls. When specific tissue stains were employed, digital images were obtained and stain density was quantified as the integrated optical density using Metamorph (Molecular Devices, Inc.; Sunnyvale, CA). Similarly, digital images were assessed with Metamorph to make all measurements of size and thickness in pixels.

Metamorph Analysis: Metamorph quantification of stain density works by converting digital slide images to bichromatic images in which the color of interest (i.e. blue when reviewing Masson's trichrome staining for collagen content) is highlighted and all other colors are eliminated. Quantification is then performed through pixel count and calculation of color density in the converted image, yielding the integrated optical density as a representation of stain density. The entire specimen can be included in one image so as to eliminate the need for calculation of multiple fields, and the software allows for calculation from a selected portion of the slide so that a region, such as the thyroarytenoid muscle, can be quantified specifically.

Trichrome staining: Five micron sections were cut from paraffin embedded larynges from radiated and control subjects. Trichrome staining was carried out according to manufacturer's guidelines (Sigma-Aldrich, St. Louis, MO). Metamorph was then employed to quantify the optical density of collagen.

Alcian blue staining for glycosaminoglycans: Duplicate sections of control and experimental samples were incubated in hyaluronidase (Sigma Aldrich, St. Louis, MO) at 37°C for 1 hour, and then sections with and without hyaluronidase digestion were stained with Alcian blue stain (pH 2.5). Sections were washed and counterstained with nuclear fast red stain. Areas containing hyaluronic acid remained unstained in digested slides and stained blue in undigested slides. Metamorph was then employed to measure the integrated optical density of hyaluronic acid.

Quantitative Histomorphometry: Histologic sections were first cut and stained with Mason's trichrome as above. These slides were used to assess gross tissue morphometry. Specimens not clearly representing the true vocal fold were excluded. Overall muscle and collagen organization were rated as normal, mildly disorganized, or severely disorganized under 10× magnification.

The thickness of the lamina propria and vocal ligament was then measured under 2× magnification. Using 40× images, muscle fiber areas were measured from 10 representative fields in the thyroarytenoid muscle from each specimen. Finally, with collagen staining blue after Mason's trichrome staining, collagen content was quantified by recording the

integrated optical density of the blue-stained collagen in both the lamina propria (2× images) and in the thyroarytenoid muscle (40× images) using Metamorph.

Additional histologic sections were then cut and stained with Alcian blue, a stain targeting hyaluronic acid as above. Hyaluronidase digestion was performed in order to confirm that tissue staining with Alcian blue represented hyaluronic acid. Superficial lamina propria hyaluronic acid content was quantified using *Metamorph* software via measurement of the integrated optical density of the blue-stained hyaluronic acid.

Immunohistochemistry: Sections were prepared for immunohistochemical staining for collagen I, collagen IV, vimentin, alpha-smooth muscle actin (α-SMA), matrix metalloproteinase 9 (MMP-9), fibronectin, and laminin.

Statistical Analysis: Once tissue analysis was complete, Microsoft Excel was used to statistically analyze the results and compare the radiated specimens to controls. For comparison, a Fisher's two-tailed t-test was performed with a p-value of 0.05 considered significant.

Microarray and RT-PCR analysis—Eight samples were prepared for microarray analysis. Out of eight samples, five passed quality control check; two control samples and two radiated vocal fold samples obtained from 1 and 2 years after radiation, and one from 10 years post radiation. Microarray data fold increase was compared between control versus 1 or 2 and 10 years after radiation.

Extraction of total RNA from lamina propria from formalin-fixed, paraffin embedded vocal folds via laser capture microdissection: Eight micron paraffin sections from control and radiated samples were dehydrated through serial passages through alcohols and xylene (Nuclease free dehydrating components from Acturus). The sections were stained by Paradise Reagent Kit (Arcturus, Mountain view, CA, USA) to visualize lamina propria. Lamina propria was then captured by laser capture micro dissection. Briefly, the micro dissection laser (PixCell Ile, Arcturus) was set to 7.5μm/45mW to isolate lamina propria. Ribonucleic acid was isolated from the lamina propria using Picopure RNA isolation kit (Arcturus). Quality check for RNA was determined using ABI taqman assay (RPL13a assay); the Ct value cut off was 30. Total RNA of 250ng was processed for Human whole genome Illumina DASL kit for micro array analysis. Two controls and three radiated specimens were subjected to complete analysis

Gene expression array analysis of formalin-fixed, paraffin embedded radiated vocal folds via whole genome cDNA-mediated annealing, selection extension, and ligation: Degraded RNA from FFPE tissue can be used in DASL, as it does not depend on intact poly-A tail for cDNA synthesis. This technology is based on highly multiplexed RT-PCR applied in a bead-microarray format. A more recent version of the method, WG-DASL capable of addressing 24,000 reference sequences, encompassing the majority of the human transcriptome, was applied radiated samples.

Whole genome-DASL and data analysis: Fold transcriptional changes of radiated samples were calculated based on control tissue values. Gene ID, Gene symbol and fold change in 1,2 and 10 years after radiation and name of the gene are provided in the corresponding tables.

Quantitative real time PCR: To confirm the microarray analysis levels of collagen-1 and fibronectin mRNA, real time PCR was employed. Evaluation for these changes began with the preparation of first strand cDNA from extracted RNA using a sensiscript kit (Qiagen,

Hilden, Germany). The real-time iCycler sequence detection system (Bio-Rad, Hercules, CA, USA) was used for the real-time reverse transcription-PCR using reverse-transcribed cDNA, human-specific primers for collagen-1, fibronectin and iQ SYBR Green Supermix (Bio-Rad). GAPDH expression was employed as a control.

Murine Vocal Fold Model

Experimental Animals—The Institutional Animal Care and Use Committee (IACUC) at a tertiary academic medical center approved the experiments described, and all experiments were conducted in accordance with the Guide for the Care and Use of Laboratory Animals, published by the U.S. Public Health Service. Mice were maintained on a 12 hour dark-light cycle and allowed free access to pelleted diet and tap water under conditions of controlled temperatures ($25 \pm 2°C$). They were humanely sacrificed by isofluorane inhalation and the larynges were immediately harvested and processed according to the methods below.

Development of murine dosing protocol—C57BL/6 mice were obtained from Jackson laboratories. Previously described protocols for murine models of lung irradiation delivered cumulative doses between 12 and 24 Gray, so the target dose was set in this range.[7,8] An initial protocol involving whole body γ-ray irradiation at a dose of 20 gray resulted in early lethality presumably due to bone marrow suppression (6 treated, 6 control). The protocol was modified to 2 doses of 8 gray and a lead shield was employed to limit radiation to the neck alone (10 treated, 10 control). Regional pigmentary change confirmed radiation localization after the first 8 gray, however 60% of mice died within a week and universal mortality was observed after the second dose of 9 gray four weeks later. Noting these mortality rates, the dosing regimen was further fractionated as previously described rat regimens demonstrated decreased weight loss, dehydration, and lethargy with such a change.[10] Ultimately, localized administration of a dosing protocol using 3 doses of 5 gray at 2 week intervals for a total dose of 15 Gray enabled animal survival after full course radiation treatment (15 treated, 15 control).

A total of 15 mice received a full course of radiation. Appropriate anesthesia was maintained using ketamine and xylazine. A custom built rodent lead cover was used to expose only the rodent neck and protect the animals from whole-body irradiation. Irradiation was administered in 3 cycles of 5 gray doses spaced 2 weeks apart. Mice were sacrificed 4 weeks after the 3rd dose. This experimental group of mice was paired with age-matched controls not receiving radiation for a total of 30 animals. Ten control and ten treated mouse larynges were harvested and fixed in formalin for histologic evaluation, and five control and five treated mouse larynges were frozen for sectioning and subsequent analysis of mRNA. Differences between irradiated and age-matched control murine larynges were blindly assessed at each time point. Histologic outcome measures include vocal fold collagen content, fibronectin content, hyaluronic acid content, and mean thyroarytenoid muscle fiber area. Transcriptional analysis for procollagen and TGF-β was then performed.

Trichrome staining—Harvested larynges from radiated and control C57B/6 mice were fixed in 4% paraformaldehyde and processed to 5μm coronal sections. Trichrome staining was carried out according to manufacturer's guidelines and following the protocol for quantification as described above for human sections.

Alcian blue staining for hyaluronic acid—Coronal sections were obtained from C57BL/6 mice as described above and subjected to the alcian blue protocol described above for the human sections. **Mean Thyroarytenoid Muscle Fiber Area**. Sections were photographed using light microscopy at 40x magnification. Using Metamorph, the mean thyroarytenoid muscle fiber area was calculated for radiated mice and controls. In a blinded

fashion, the pixel area of 10 representative muscle fibers was measured in each section. The mean muscle fiber area was then calculated for each of 10 radiated mice and 10 control mice.

Immunohistochemistry—Immunohistochemical staining of fibronectin was carried out using the Vectastain ABC kit (Vector Laboratories) according to the manufacturer's protocol. Briefly, primary rabbit anti-mouse fibronectin antibody, 1:500 dilution (Santa cruz biotechnology, CA) was applied to deparaffinized and rehydrated tissue sections prior to overnight incubation at 4°C. Enzyme-conjugated secondary antibodies were applied, and the specific staining was visualized after the addition of the enzyme-specific diaminobenzidine substrate and hematoxylin counterstaining.

Extraction of total RNA from lamina propria from formalin-fixed, paraffin embedded vocal folds via laser capture microdissection: Larynges from radiated and control mice were harvested and embedded in OCT (optimal cut temperature) to obtain frozen sections. Using a cryotome, 8 μm sections were cut under a RNAse-free environment and stored at −80°C until further processing. These cryosections were dehydrated through serial passages of alcohols and xylene and then stained using the Histogene LCM staining kit (Arcturus, Mountain view, CA, USA) to visualize the vocal folds. The protocol described above for the human sections was employed.

Quantitative real time PCR—Increased collagen content is a prominent component of fibrosis, and previous *in vivo* experiments have demonstrated a significant increase in TGF-β expression in irradiated lung tissue.[11,12] Preparation of first strand cDNA from extracted RNA was performed using the Sensiscript kit (Qiagen, Hilden, Germany). The real-time iCycler sequence detection system (Bio-Rad, Hercules, CA, USA) was used for the real-time reverse transcription-PCR using reverse-transcribed cDNA, murine gene-specific primers for procollagen (sense: GTGCTGTTGGTGCTGCTG, antisense: CCGGCCCTGATGGAAAC) and TGF-β (Sense: ATTCCTGGCGTTACCTTGG, Antisense: CCTGTATTCCGTCTCCTTGG), and iQ SYBR Green Supermix (Bio-Rad). GAPDH (sense: TCAACGGCACATACTCAGC, antisense: ACTCCACCACATACTCAGC) expression levels were used as a reference, and procollagen and TGF-β mRNA levels were measured.

G. Statistical analysis—Statistical analysis was performed by means of Student's *t* test (Prism 4.0; Graph PAD, San Diego, CA, USA). A probability value of $p < 0.05$ was regarded as significant.

RESULTS

Human Vocal Fold Studies

In all, 20 radiated vocal folds from 13 patients were evaluated. Fourteen were from seven patients who had no history of true glottal disease. Six were included from the uninvolved side of patients with a history of contralateral glottal disease. For the purposes of statistical analysis, only one vocal fold was included from those patients in which both vocal folds were free of primary disease, leaving a total of 13 radiated vocal folds from 13 separate patients.

A mean of 30 months (+/−12 months) elapsed between completion of radiation and laryngectomy (Table 1). All patients had previously received radiation with curative intent. Specific records regarding the exact radiation fields and dosage administration were not consistently available due to administration of treatment at multiple radiation centers over a

broad time period, however as all patients completed treatment, it can be assumed that each received a dosage in the commonly accepted therapeutic range of 66 and 70 gray. Similarly, sufficient records regarding a history of induction or concurrent chemotherapy were lacking.

Blinded morphometric analysis revealed increased collagen and muscle fiber disorganization in radiated specimens—Blinded analysis of Mason's trichrome stained slides revealed increased collagen and muscle fiber disorganization in radiated specimens versus controls (Figure 1). All 3 controls were rated as having normal morphometry. Of the radiated vocal folds, 3 were rated as morphometrically normal, 9 as mildly disorganized, and 8 as severely disorganized.

Thyroarytenoid muscle collagen content was significantly increased in radiated specimens—Metamorph analysis of trichrome slides to quantify collagen content in the thyroarytenoid muscle revealed a significant increase in collagen in radiated specimens vs. controls (n=12, p=0.011; Figure 2).

Superficial lamina propria collagen content was significantly increased in radiated specimens—Metamorph analysis of trichrome slides to quantify collagen content in the superficial lamina propria revealed a significant increase in collagen in radiated specimens vs. controls (n=13, p=0.0007; Figure 3).

Superficial lamina propria hyaluronic acid content was not significantly increased in radiated specimens—Metamorph analysis of Alcian blue slides to quantify hyaluronic acid content in the superficial lamina propria revealed an increase in hyaluronic acid content in radiated specimens, however this increase failed to achieve statistical significance (n=13, p=0.087).

Thyroarytenoid muscle laminin content was significantly decreased in radiated specimens—Metamorph analysis of laminin demonstrated a significant decrease in laminin content in radiated specimens compared to controls (n=13, p < 0.0001; Figure 4).

Superficial lamina propria fibronectin content was significantly increased in radiated specimens—Metamorph analysis of fibronectin demonstrated a significant increase in fibronectin content in radiated specimens compared to controls (n= 2, p = 0.021; Figure 5).

Thyroarytenoid muscle and superficial lamina propria matrix metalloproteinase–9 content was not significantly different in radiated and control specimens—Metamorph analysis MMP-9 demonstrated increased MMP-9 content in the thyroarytenoid muscle of radiated specimens compared to controls. However this increase failed to achieve statistical significance (n=12, p = 0.17). MMP-9 content of the superficial lamina propria was also not significantly different (n = 13, p = 0.83).

Superficial lamina propria vimentin content was not significantly different in radiated and control specimens—*Metamorph* analysis of vimentin revealed no significant difference in the SLP vimentin content between radiated and control specimens (n=13, p=0.90).

Poor immunostaining for collagen I, collagen IV, α-SMA, SLP laminin, thyroarytenoid muscle fibronectin, and thyroarytenoid muscle vimentin was

noted—The specimens did not stain avidly for these targets. Quantification was not performed.

Mean muscle fiber area did not differ significantly between the radiated and control specimens—Metamorph software was used to quantify the mean muscle fiber area of the thyroarytenoid muscle in radiated and control specimens. The mean area was decreased in radiated specimens, however this change was not statistically significant (n=12, p=0.35). Muscle fiber area did appear much more variable in the radiated specimens.

No significant difference was noted in the thickness of the superficial lamina propria or the vocal ligament in radiated and control specimens—Metamorph software was used to quantify the thickness of the superficial lamina propria (SLP) and the vocal ligament in radiated and control specimens. Mean SLP (n=13, p=0.85) and vocal ligament (n=13, p=0.31) thickness were slightly decreased in radiated specimens, however these differences failed to achieve statistical significance.

SLP Collagen increased significantly in radiated specimens with a longer time interval between completion of radiation and resection—Subgroup analysis was performed for collagen content in radiated thyroarytenoid muscle and SLP specimens, as well as SLP fibronectin and muscle laminin content (i.e. all those variables demonstrating a significant difference between radiated and control specimens). To assess the impact of time after radiation on the changes in the extracellular matrix, radiated specimens were divided into those obtained less than 12 months after completion of treatment and those obtained greater than 12 months after completion of treatment. SLP collagen content was significantly greater 12 months or more after completion of radiation therapy (p=0.03). Thyroarytenoid muscle collagen, SLP fibronectin, and muscle laminin content were not significantly different between the two groups.

Microarray analysis—Transcriptional changes between human irradiated on non-irradiated lamina propria at years 1–2 and year 10 following treatment were assessed using whole-genome microarray. Gene clusters most relevant to fibrosis were selected for analysis, including collagens, matrix metalloproteinases, glycosaminoglycans, fibronectins, laminins, and genes related to inflammation, oxidative stress, and apoptosis. Data regarding fold changes of specific genes within these clusters are presented in the Appendix Tables 1 – 7. In summary, significant differences were observed with regard to collagen transcription, both early and late following irradiation. Decreased matrix metalloproteinase expression was also noted at years 1–2, and year 10. Fibronectin transcription increased significantly, while laminin transcription decreased. Genes in the proinflammatory cluster (interleukins, and tumor necrosis factors) also increased significantly both early and late following irradiation. Similarly, genes related to oxidative stress and apoptosis increased significantly.

RT-PCR results: Radiated human vocal folds demonstrate significantly higher levels of collagen-1 and fibronectin mRNA: Transcriptional levels of collagen-1 and fibronectin were assessed as key factors of fibrosis, and to confirm findings noted on microarray. Collagen and fibronectin levels were compared between radiated and non-irradiated sections and expressed as fold change over untreated samples. Significantly increased collagen-1 (n=4, *P<0.01), and fibronectin expression (n=4 *P<0.03) were observed in radiated human vocal folds compared to controls (Figures 6, 7, 8).

Part 2: Murine Vocal Fold Model

Radiation was successfully localized to cervical region as demonstrated by depigmentation at the exposed site—A customized lead-shield successfully

prevented the mortality associated with whole-body irradiation. Mice maintained adequate health and maintained weight appropriately. Radiation led to depigmentation and alopecia in the irradiated field. (Figure 9).

Increased collagen content was observed in radiated murine vocal folds—
Collagen density in vocal folds was assessed via trichrome staining. Collagen content, quantified using Metamorph software, was significantly higher in the lamina propria and thyroarytenoid muscle of radiated mice when compared to controls (n=8, p<0.002) (Figure 10).

Hyaluronic acid concentrations were not altered following radiation in the mouse vocal fold—Hyaluronic acid content was assessed in radiated mice using Alcian blue staining. Staining density trended higher in the radiated specimens, however, this trend did not achieve statistical significance. (n=8, p=0.82; Figure 11).

Mean thyroarytenoid muscle fiber area was not significantly different between radiated and control mice—In order to assess radiation induced damage to thyroarytenoid muscle fibers, muscle fiber area was measured in the radiated thyroarytenoid muscle. The mean pixel area for radiated mice was 3564, and for control mice was 4110 (p=0.61). Although the thyroarytenoid muscle architecture in radiated mice appeared grossly altered with distortion of individual muscle fibers, differences in fiber area were not significant.

Radiated mice demonstrate significantly higher levels of fibronectin—
Radiation-induced alterations in extracellular matrix and fibrous protein content including fibronectin were assessed via immunohistochemistry. Fibronectin content was significantly higher in radiated versus control mice (n=4, p<0.02; Figure 12).

Radiation induced increases in procollagen and TGF-β mRNA—Transcriptional levels of procollagen and TGF-β, key factors in fibrosis, were determined. Procollagen and TGF-β expression was compared between radiated and non-radiated sections. Real-time PCR confirmed significantly increased procollagen (n=5, p=0.048) and TGF-β mRNA (n=5, p=0.007) in radiated murine larynges versus controls (Figure 13).

Human and mouse vocal fold radiation fibrosis correlation

Similar changes were observed in radiated human vocal folds and our murine model of vocal fold irradiation. Increased collagen transcription and translation were noted on histomorphometry and RT-PCR. Fibronectin was also produced and deposited at increased levels in the lamina propria of both human and murine vocal folds. Surprisingly, little differences in hyaluronic acid concentration were observed in radiated vocal fold tissue in either of our models.

DISCUSSION

The clinical effects of radiation on laryngeal function, and in particular the voice, can be profound. Radiation is known to induce a fibroblastic response throughout the radiated field yielding a significant decrease in vocal fold pliability. Although the oncologic response to this treatment is highly effective and allows for laryngeal preservation, patients often suffer from severe dysphonia, vocal strain, and impaired communication resulting in decreased post-treatment quality of life.[1]

Advances in the delivery of radiation, such as intensity-modulated radiation therapy, have improved the precision of radiation.[13] Although these advances allow for increased dose delivery to desired targets while minimizing irradiation to surrounding tissue, the post-treatment effects on the irradiated tissue persist. Currently few effective strategies exist to prevent these changes or ameliorate their progression after therapy.

In order to develop strategies to prevent and treat radiation fibrosis in the human vocal fold, more detailed understanding of the molecular changes that occur in these tissues is needed. The aims of the current studies were to define fundamental changes occurring in the human vocal fold following radiation, and then to develop a mouse model of radiation-induced vocal fold fibrosis that parallels the changes seen in the human. The development of this murine model will facilitate further characterization of vocal fold radiation fibrosis and will allow for a platform to study strategies to prevent and treat fibrosis that occurs in the vocal fold following radiation. To better understand the rationale for the design of this study it is important to appreciate the basic concepts of radiation therapy and the effects it has on human tissue. Presented here is a brief review of the current literature on the mechanism of action of radiation therapy and both the acute and late manifestations seen in response to ionizing radiation.

Radiation Physics

The term radiation broadly refers to any form of energy moving through a medium. In medicine the two types of energy used are either electromagnetic energy, for example gamma rays and x-rays, or particle energy, such as protons, electrons or neutrons. In radiation oncology, electromagnetic radiation, particularly x-ray, is more commonly used due to its ability to traverse the skin and deposit energy deep into tissues.[13] Gamma rays are used in brachytherapy, while particle radiation, specifically electron radiation, is used to treat pathologies on skin surfaces, due to its decreased ability to penetrate skin. Novel approaches using particle radiation in the form of protons and neutrons have been introduced in the past two decades, but have not shown clinical superiority to electromagnetic radiation.

In addition to the type of energy used, radiation can be broken down into either ionizing or non-ionizing radiation. Ionizing radiation, typically radiation above 125eV of energy, has energy sufficient to raise an atom's outer electron to a higher energy state. When this electron returns to its natural state it releases energy. Radiation used in cancer treatment relies on ionizing radiation, discussed in the following sections. Although the unit eV (electron volts) quantifies the amount of energy in radiation, clinically, radiation is measured in terms of the amount of energy absorbed. The current unit of radiation is Grays, equivalent to Joules per kilogram. One gray is equal to 100 rads, which was the previously used unit of measurement.[14]

Mechanisms of Radiation Injury

The energy released when ionized electrons return to their natural energy state allows radiation to damage individual cellular components. Historically, it was thought that the mechanism of radiation-induced injury was related solely to DNA damage.[15] The energy released when ionized electrons return to their natural state is enough to break chemical bonds, including those of DNA. Although single stranded breaks are easily repaired by cellular mechanisms, double stranded breaks require more complex repair systems and can accumulate and inhibit the mitotic capacity of cells, ultimately leading to cell death though apoptosis.[14,15] Over the past two decades, other mechanisms have been proposed including the formation of reactive oxygen species (ROS) via the ionization of O_2 and H_2O.[16,17] In addition, radiation has been shown to activate multiple cytokine-mediated cellular signaling pathways.[16,17] These pathways are thought to be activated by a combination of oxidation

from the formation of ROS and sub-lethal DNA damage, and are proposed to mediate apoptosis[18,19] (p53[17,20], ataxia telangiectasia mutation[17], and ceramide[15]) and yield changes in cellular function and production of cytokines which are responsible for the multitude of late clinical effects seen in radiation.[16,21–26]

These two mechanisms of cellular damage, DNA damage and activation of cellular signaling, provide insight into the relative sensitivity and mechanisms of radiation-induced tissue damage. The role of DNA fragmentation in radiation treatment explains why cells in the G2 and M phase of mitosis are most susceptible to radiation.[22] Furthermore this explains why radiation has a greater sensitivity for rapidly dividing tumor cells, and explaining why organs with high turnover rates, such as the testes and mucosa, are more susceptible to radiation effects than those with low turnover rates, such as bone.[14] The role of ROS provides rational for the radioprotective effects of hypoxia. Without sufficient O_2, the amount of ROS is decreased, leading to a decrease in cellular damage, a problem in solid tumors, which often outgrow their vasculature.[15] Finally, the activation of multiple signaling pathways by ROS is thought to explain the wide variety of long-term effects seen in irradiated tissues.

Late Effects of Radiation in Non-Laryngeal Tissues

The effects of radiation are not limited to the acute cell death caused by DNA breaks and apoptosis. Late effects of radiation, seen months and years after treatment, has become a major healthcare issue as the number of cancer patients surviving for extended periods of time after treatment has drastically increased over time, with over 60% of adults and 70% of children surviving greater than 5 years.[16] Late effects of radiation are varied and can greatly depend on the tissue being irradiated. Common late effects seen are tissue edema, xerostomia, skin pigmentation changes, alopecia, telangiectasia, tissue atrophy, tissue contracture, ulcer, necrosis, and fibrosis. For the purposes of this study, fibrosis and current understandings of its pathogenesis and treatment are discussed.

Radiation-induced fibrosis is the excess accumulation of extracellular matrix component proteins yielding reduced tissue compliance. In the lung, fibrosis causes decreased tissue elasticity as well as decreased gaseous diffusion in the alveoli, both of which lead to impaired oxygenation. In the heart, fibrosis causes restrictive heart disease. In hollow organs such as the GI tract or hepatic ducts, radiation fibrosis results in strictures. Blood vessels also undergo fibrosis with resultant intimal hyperplasia as well was decreased diffusion in capillary beds. Although fibrosis may occur in most sites, the central nervous system, bone and marrow do not appear susceptible to these fibroblastic alterations. Our understanding of the mechanisms involved in radiation-induced fibrosis has changed over the years. Current theories on the pathogenesis of radiation fibrosis involve multiple cellular pathways and signaling molecules all converging to induce fibrosis. The most studied of these is Transforming Growth Factor Beta (TGF-*B*). TGF-B has 5 sub-families, but TGF-B1 has been implicated in fibrosis. ROS formed from radiation are able to activate TGF-B1 from their inactive latent phase. TGF-B1 acts through Smad signaling proteins to induce transcription of pro-collagens, and potentially more important, the Smad-mediated TGF-B signaling is thought to induce fibroblast differentiation to myofibroblasts. Myofibroblasts, which are alpha smooth muscle actin positive fibroblasts (a-SMA), are central components of ECM formation and produce collagen, fibronectin, elastin, hyaluronic acid, and matrix metalloprotiens. The activation of myofibroblasts is thought to be a key component of fibrosis formation.[22] Increased TGF-B has been shown in irradiated rectum tissue up to 40 weeks post radiation, as well as concomitant increase in Collagen I III.[26] Increased TGF-B has also been implicated in radiation enteritis.[22] Mouse models of radiation have also shown increases in TGF-B in response to radiation.[21,24] Another protein implicated in radiation fibrosis is connective tissue growth factor (CTFG). CTGF is induced by ROS and is

involved in the TGF-B feedback loop. CTGF is thought to function as a continual stimulus for increased TGF-B levels, even after the oxidative stress of ROS has decreased. CTGF mRNA and protein levels have been shown to be increased in patients undergoing bowel resection for obstruction following pelvic radiation.[26]

Radiation's effect on blood vessel thrombomodulin (TM) levels has also been implicated in fibrosis. TM is a potent anticoagulant and TM levels in vessels decreased in response to ionizing radiation, leading to the accumulation of thrombin-induced release of TGF-B from platelets. TM levels are further depleted leading to a cycle of increased TGF-B and fibrosis. Decreased TM is thought to increase hypoxia in radiated organs, a potential secondary etiology for fibrosis.[26]

Alterations of the Renin Angiotensinogen System (RAS) have also been implicated in radiation fibrosis. Angiotensinogen II (Ang II) has been shown to mediate late effects seen in radiation such as fibrosis, as evidenced by the protective effects of ACE Inhibitors and ARBs treatment at levels below their hypertensive dosage. It is believed that radiation activates intra-organ RAS to produce Ang II. The exact mechanism of Ang II on fibrosis is unknown, but current hypotheses view it as either increasing TGF-B production or mediating a state of chronic inflammation.[25,26]

Comparison of Late Effects in Non-Laryngeal Tissue Versus Laryngeal Tissue

Although there are a large number of studies examining late effects of radiation in many anatomical sites, few have investigated the late effects seen in laryngeal tissue. Most late effects in the larynx do not occur until at least three months post radiation due to the long-standing hypovascularity following treatment.[27] It is well documented in the literature that laryngeal radiation can have serious impacts on voice quality.[28–30] Common late effects are persistent laryngeal edema and fibrosis, but radionecrosis of the larynx, although rare, is a feared complication, which has been reported to occur up to 50 years post treatment.[27,31]

Because vocal fold fibrosis is most commonly caused by mechanisms other than radiation, there is a large body of literature investigating vocal fibrosis as a result of surgical scarring. These studies have shown in increase inflammatory markers, TGF-B, procollagen and MMPs in response to vocal fold damage, and a subsequent decrease in hyaluronic acid and the organization of collagen.[28,30,32] The lack of animal models for radiation of the vocal folds has limited the research on radiation induced fibrosis. The few studies that have examined radiation fibrosis have showing increases in ROS, TGF-B and MMPs within an hour of treatment, but with only limited studies with small sample sizes, further investigation is warranted.[10] Although the time course for assessment of chronic fibrosis in the murine model proposed herein is relatively short (4 weeks from completion of radiation to assessment), chronic fibrotic changes in the pulmonary tissue of mice occur over a similar timeframe, lending support to the validity of this model.[8,9]

The current study sought to provide increased insight into the effects radiation on the cellular level. By examining transcriptional and translational changes, we were able to investigate each stage of the response to radiation. Our data show increased transcription, translation and protein levels of collagen and fibronectin in response to radiation. Laminin was decreased in both protein content and transcription. Finally, matrix metalloproteinases decreased, while markers of inflammation, apoptosis and oxidative stress increased. Furthermore, we observed increased collagen as the duration of time from treatment increased. In addition, this increased collagen content was significant less organized. These changes were consistent with previous studies in other tissue systems. However, decreased matrix metalloproteinase observed in the current is not consistent with the majority of previous investigation regarding radiation-induced fibrosis.

Radiation-Induced Fibrosis and Vocal Fold Physiology

Phonation involves significant coordination in order to produce normal pitch, quality, loudness, and flexibility.[33,34] The lungs are the power source to produce adequate expiratory flow to generate phonation. Fortunately, in the absence of pulmonary pathology otherwise, advanced radiation therapy techniques rarely impact pulmonary flow post treatment. Next, adequate neuromuscular function in the larynx is required first and foremost to provide complete glottal closure to resist subglottal airflow and set the stage for vocal fold vibration. This requires intact neuromuscular integrity to the intrinsic muscles of the larynx and fully mobile cricoarytenoid joints. The current study demonstrated that radiation fibrosis in the vocal fold leads to increased collagen production, deposition, and possibly impaired remodeling within the thyroarytenoid muscle itself. Furthermore, reduction in laminin translation in the muscle may lead to loss of muscle cell fiber integrity and contractile dysfunction. Loss of adequate vocal fold closure leads to loss of laryngeal resistance to subglottal airflow and air escape during phonation that presents clinically with reduced vocal fold volume, increased breathiness, and reduced vocal endurance.

Beyond complete glottal closure, the periodic vocal fold vibration that leads to stable sound generation requires both normal vocal fold cover and body volume and pliability. Although no changes were seen in absolute vocal fold body or cover volume in the human or the mouse following radiation in these data, notable changes occurred in both that could affect vocal fold and body pliability. In both the mouse and human, the superficial lamina propria contained increases in collagen deposition and disordered collagen organization. Furthermore, the superficial lamina propria was noted to have significant increases in fibronectin. Elevated collagen deposition in the thyroarytenoid muscle may contribute to stiffness of the vocal fold body. These changes likely contribute to impaired vocal fold pliability and the vibratory characteristics seen clinically in patients following radiation.

Additionally, vocal fold stiffness may contribute to pitch perturbations in patients with post-radiation fibrosis. Stiffness of the vocal fold typically leads to an abnormally high pitched voice. Flexibility of voice in dynamic speaking and singing requires precise modulation of vocal fold length, tension and shape. The fibrotic changes noted in the human superficial lamina propria and thyroarytenoid muscle can be implicated in impairing flexibility in voice production. Collectively, radiation fibrosis likely can impair vocal fold closure, pliability, and dynamic changes in tension and length. These changes lead to loss of vocal volume and quality, vocal breathiness, pitch perturbations, and reduced vocal flexibility.

Potential Preventative and Therapeutic Targets for Radiation-Induced Vocal Fold Fibrosis

Although radiation fibrosis of the vocal folds is significant, there has been a long history of attempts at preventing and treating this condition. Due to the large morbidity it can impart on patient's lives there have been a wide variety of approaches to treat vocal fold fibrosis. Due to the complex interplay between cell signaling, cytokines and the extracellular matrix there are a vast array of potential treatment targets.

Currently there are many approaches being investigated for vocal fold scar, which may be applicable for radiation fibrosis. Injectable biogels have shown the ability to decrease scar formation in in-vivo models. Treatment of these biogels with Tumor Necrosis Factor Alpha (TNF-a) has been shown to also decrease vocal fold synthesis of collagen III, fibronectin and MMPs.[35] Collagen injections in combination with CO_2 laser treatment of the scar have been shown to increase glottal competence.[36] Other forms of laser, such as pulse dye laser, have also been used to attempt to treat vocal fibrosis.[37] Hepatocyte Growth Factor injected via microtubules has shown to *decrease* procollagen production in mouse models.[38] Autologous fibroblasts have been injected into vocal folds and have shown to improve

mucosal wave and patients Voice Handicap Index.[39] Laryngeal steroid injections have been used in the past, but data on the efficacy this approach is mixed.[40] Hyaluronic acid preparations, applied acutely following injury have also to decreased fibrosis in animal models.[39]

Validity and Utility of a Murine Model of Radiation-Induced Vocal Fold Injury

Established murine models exist for vocal fold scarring and vocal fold aging.[7] Although fibrotic changes are evident in both conditions, the inciting factor is markedly different and the underlying pathophysiology cannot be presumed equal. Similarly, research findings, and in particular therapeutic modalities, found effective in the treatment of these conditions cannot necessarily be translated to the radiated vocal fold. Likewise, although there are established animal models for radiation fibrosis at other anatomical sites there is surprisingly little literature on animal models for radiation in laryngeal tissues.[41,42] Recently, a rat model has been studied for investigating radiation effects on the vocal folds. A radiation dosing protocol was successfully identified allowing for survival. After 12 weeks, Histomorphmetric analysis of the vocal folds demonstrated substantial epithelial hypertrophy and primitive fibrosis.[10] The mouse model presented here builds on this important work providing initial transcriptional or translation analysis of proteins involved in inflammation or fibrosis.

A tolerable technique and schedule of radiation has been defined with minimal murine mortality. Statistically-significant histologic changes observed include increased collagen density and fibronectin content in the lamina propria and thyroarytenoid muscle. Hyaluronic acid content appeared grossly increased however did not reach statistical significance between radiated and control animals. Transcriptional analysis further demonstrated a significant difference between radiated and control animals, with increased procollagen and TGF-β mRNA.

These histologic changes are consistent with our preliminary data examining histologic changes in irradiated human vocal fold tissue. Similar changes include increased collagen content in the lamina propria and thyroarytenoid muscle as well as significant alterations to the histologic structure. Transcriptional increases in collagen were also seen in both models. Increased fibronectin was observed in both mouse and human tissue. Interestingly, no changes in hyaluronic acid levels, a major extracellular component of the lamina propria, were seen in either model. Other strengths of our murine model include wide availability, reduced cost, and the availability of transgenic strains.

Establishment of this model will enable further characterization of the pathophysiology of radiation-induced laryngeal fibrosis. With the known fibrotic reaction in human radiated vocal folds, further evaluation to translate findings in this model to humans should prove extremely valuable. Future studies will employ this model to assess both preventive and therapeutic interventions to treat this potentially devastating consequence of a necessary oncologic treatment.

Conclusion

Radiation fibrosis is a complex phenomenon and our understanding of the mechanisms and molecular events and our understanding of the underlying etiologies is poor. Data from the current study provide preliminary insight into these complex processes. Further investigation is required both in human tissue and in any potential model to enhance our knowledge further. Nonetheless, this study is the first in demonstrating basic molecular changes that occur in human vocal fold tissue following irradiation. Additionally, the mouse model developed herein parallels many of the findings seen in human vocal folds following

radiation and can serve as a tool to study further events leading to radiation fibrosis as well as potential preventive and therapeutic modalities for the problem.

Acknowledgments

REFERENCES

1. Fung K, Lyden TH, Lee J, et al. Voice and swallowing outcomes of an organ-preservation trial for advanced laryngeal cancer. Int J Radiat Oncol Biol Phys. 2005; 63:1395–1399. [PubMed: 16087298]

2. Mendenhall WM, Parsons JT, Buatti JM, Stringer SP, Million RR, Cassisi NJ. Advances in radiotherapy for head and neck cancer. Semin Surg Oncol. 1995; 11:256–264. [PubMed: 7638513]

3. Fung K, Yoo J, Leeper HA, et al. Vocal function following radiation for non-laryngeal versus laryngeal tumors of the head and neck. Laryngoscope. 2001; 111:1920–1924. [PubMed: 11801970]

4. Hirano S, Bless DM, del Rio AM, Connor NP, Ford CN. Therapeutic potential of growth factors for aging voice. Laryngoscope. 2004; 114:2161–2167. [PubMed: 15564837]

5. Hirano S, Nagai H, Tateya I, Tateya T, Ford CN, Bless DM. Regeneration of aged vocal folds with basic fibroblast growth factor in a rat model: a preliminary report. Ann Otol Rhinol Laryngol. 2005; 114:304–308. [PubMed: 15895786]

6. Kang SK, Rabbani ZN, Folz RJ, et al. Overexpression of extracellular superoxide dismutase protects mice from radiation-induced lung injury. Int J Radiat Oncol Biol Phys. 2003; 57:1056–1066. [PubMed: 14575837]

7. Kolachala VL, Torres-Gonzalez E, Mwangi S, et al. A senescence accelerated mouse model to study aging in the larynx. Otolaryngol Head Neck Surg. 2010; 142:879–885. [PubMed: 20493362]

8. Rube CE, Uthe D, Schmid KW, et al. Dose-dependent induction of transforming growth factor beta (TGF-beta) in the lung tissue of fibrosis-prone mice after thoracic irradiation. Int J Radiat Oncol Biol Phys. 2000; 47:1033–1042. [PubMed: 10863076]

9. Katoh H, Ishikawa H, Hasegawa M, et al. Protective Effect of Urinary Trypsin Inhibitor on the Development of Radiation-Induced Lung Fibrosis in Mice. J Radiat Res (Tokyo). 2010

10. Saltman B, Kraus DH, Szeto H, et al. In vivo and in vitro models of ionizing radiation to the vocal folds. Head Neck. 2010; 32:572–577. [PubMed: 19672960]

11. Park KJ, Oh YT, Kil WJ, Park W, Kang SH, Chun M. Bronchoalveolar lavage findings of radiation induced lung damage in rats. J Radiat Res (Tokyo). 2009; 50:177–182. [PubMed: 19377267]

12. Movsas B, Raffin TA, Epstein AH, Link CJ Jr. Pulmonary radiation injury. Chest. 1997; 111:1061–1076. [PubMed: 9106589]

13. Heron DE, Godette KD, Wynn RA, et al. Radiation medicine innovations for the new millenium. J Natl Med Assoc. 2003; 95:55–63. [PubMed: 12656450]

14. Eisbruch A, Lichter AS. What a surgeon needs to know about radiation. Ann Surg Oncol. 1997; 4:516–522. [PubMed: 9309344]

15. Ross GM. Induction of cell death by radiotherapy. Endocr Relat Cancer. 1999; 6:41–44. [PubMed: 10732785]

16. Zhao W, Diz DI, Robbins ME. Oxidative damage pathways in relation to normal tissue injury. Br J Radiol. 2007; 80(Spec No 1):S23–S31. [PubMed: 17704323]

17. Valerie K, Yacoub A, Hagan MP, et al. Radiation-induced cell signaling: inside-out and outside-in. Mol Cancer Ther. 2007; 6:789–801. [PubMed: 17363476]

18. Dent P, Yacoub A, Fisher PB, Hagan MP, Grant S. MAPK pathways in radiation responses. Oncogene. 2003; 22:5885–5896. [PubMed: 12947395]

19. Kim R. Recent advances in understanding the cell death pathways activated by anticancer therapy. Cancer. 2005; 103:1551–1560. [PubMed: 15742333]

20. Lindsay KJ, Coates PJ, Lorimore SA, Wright EG. The genetic basis of tissue responses to ionizing radiation. Br J Radiol. 2007; 80(Spec No 1):S2–S6. [PubMed: 17704322]

21. Herskind C, Bamberg M, Rodemann HP. The role of cytokines in the development of normal-tissue reactions after radiotherapy. Strahlenther Onkol. 1998; 174(Suppl 3):12–15. [PubMed: 9830449]

22. Nguyen NP, Antoine JE, Dutta S, Karlsson U, Sallah S. Current concepts in radiation enteritis and implications for future clinical trials. Cancer. 2002; 95:1151–1163. [PubMed: 12209703]

23. Panizzon RG, Hanson WR, Schwartz DE, Malkinson FD. Ionizing radiation induces early, sustained increases in collagen biosynthesis: a 48-week study in mouse skin and skin fibroblast cultures. Radiat Res. 1988; 116:145–156. [PubMed: 3186926]

24. Randall K, Coggle JE. Expression of transforming growth factor-beta 1 in mouse skin during the acute phase of radiation damage. Int J Radiat Biol. 1995; 68:301–309. [PubMed: 7561390]

25. Wynn TA. Cellular and molecular mechanisms of fibrosis. J Pathol. 2008; 214:199–210. [PubMed: 18161745]

26. Yarnold J, Brotons MC. Pathogenetic mechanisms in radiation fibrosis. Radiother Oncol. 2010; 97:149–161. [PubMed: 20888056]

27. Cukurova I, Cetinkaya EA. Radionecrosis of the larynx: case report and review of the literature. Acta Otorhinolaryngol Ital. 2010; 30:205. [PubMed: 21253286]

28. Hansen JK, Thibeault SL. Current understanding and review of the literature: vocal fold scarring. J Voice. 2006; 20:110–120. [PubMed: 15964741]

29. Waghmare CM, Agarwal J, Bachher GK. Quality of voice after radiotherapy in early vocal cord cancer. Expert Rev Anticancer Ther. 2010; 10:1381–1388. [PubMed: 20836673]

30. Bless DM, Welham NV. Characterization of vocal fold scar formation, prophylaxis, and treatment using animal models. Curr Opin Otolaryngol Head Neck Surg. 2010; 18:481–486. [PubMed: 20962643]

31. Fitzgerald PJ, Koch RJ. Delayed radionecrosis of the larynx. Am J Otolaryngol. 1999; 20:245–249. [PubMed: 10442778]

32. Allen J. Cause of vocal fold scar. Curr Opin Otolaryngol Head Neck Surg. 2010; 18:475–480. [PubMed: 20861796]

33. Sundberg J, Titze I, Scherer R. Phonatory control in male singing: a study of the effects of subglottal pressure, fundamental frequency, and mode of phonation on the voice source. Journal of voice : official journal of the Voice Foundation. 1993; 7:15–29. [PubMed: 8353616]

34. Titze IR. Current topics in voice production mechanisms. Acta Otolaryngol. 1993; 113:421–427. [PubMed: 8517148]

35. Chen X, Thibeault SL. Role of tumor necrosis factor-alpha in wound repair in human vocal fold fibroblasts. Laryngoscope. 2010; 120:1819–1825. [PubMed: 20715091]

36. Martinez Arias A, Remacle M, Lawson G. Treatment of vocal fold scar by carbon dioxide laser and collagen injection: retrospective study on 12 patients. Eur Arch Otorhinolaryngol. 2010; 267:1409–1414. [PubMed: 20306066]

37. Prufer N, Woo P, Altman KW. Pulse dye and other laser treatments for vocal scar. Curr Opin Otolaryngol Head Neck Surg. 2010; 18:492–497. [PubMed: 20842035]

38. Kolachala VL, Berg EE, Shams S, et al. The use of lipid microtubes as a novel slow-release delivery system for laryngeal injection. Laryngoscope. 2011; 121:1237–1243. LID-1210.1002/lary.21796 [doi]. [PubMed: 21480281]

39. Chhetri DK, Mendelsohn AH. Hyaluronic acid for the treatment of vocal fold scars. Curr Opin Otolaryngol Head Neck Surg. 2010; 18:498–502. [PubMed: 20856119]

40. Mortensen M. Laryngeal steroid injection for vocal fold scar. Curr Opin Otolaryngol Head Neck Surg. 2010; 18:487–491. [PubMed: 21045693]

41. Degryse AL, Lawson WE. Progress toward improving animal models for idiopathic pulmonary fibrosis. Am J Med Sci. 2011; 341:444–449. [PubMed: 21613932]

42. Thanik VD, Chang CC, Zoumalan RA, et al. A novel mouse model of cutaneous radiation injury. Plast Reconstr Surg. 2011; 127:560–568. [PubMed: 21285760]

APPENDIX: MICROARRAY RAW DATA

Numbers indicate expression fold change up or down (−) from control

Table 1

a: Housekeeping gene controls		
Gene ID	**House keeping genes**	**Fold change**
ILMN_1802252	GAPDH	1.12103
ILMN_2152131	β-actin	1.14968

a Fibrous proteins collagens						
Years after treatment		**1&2**	**1&2**	**10**	**10**	
Gene ID	**Gene Symbol**	**up**	**down**	**up**	**down**	
ILMN_1751161	COL7A1	8.5		4.0		collagen, type VII, alpha 1
ILMN_1792736	COL21A1	4.6		5.1		collagen, type XXI, alpha 1
ILMN_1701308	COL1A1	2.5				collagen, type I, alpha 1
ILMN_1789507	COL11A1	2.5		2.8		collagen, type XI, alpha 1
ILMN_2311456	COL11A2			2.3		collagen, type XI, alpha 2
ILMN_1685122	COL9A2	2.4				collagen, type IX, alpha 2
ILMN_2370624	COL13A1	2.4				collagen, type XIII, alpha 1
ILMN_1684554	COL16A1	2.2				collagen, type XVI, alpha 1
ILMN_1788377	COL27A1	2.2				collagen, type XXVII, alpha 1
ILMN_1733756	COL12A1	2.2				collagen, type XII, alpha 1
ILMN_2402392	COL8A1	2.1				collagen, type VIII, alpha 1
ILMN_1742534	COL4A5	2.0		3.2		collagen, type IV, alpha 5
ILMN_1778308	COL4A4	2.0		2.0		collagen, type IV, alpha 4
ILMN_1662731	COL4A3			3.9		collagen, type IV, alpha 3
ILMN_1773079	COL3A1	2.0		2.1		collagen, type III, alpha 1
ILMN_1651282	COL17A1	2.0				collagen, type XVII, alpha 1
ILMN_1666665	COL23A1			2.0		collagen, type XXIII, alpha 1

c: Matrix Metalloproteinases						
Years after treatment		**1&2**	**1&2**	**10**	**10**	
Gene ID	**Gene Symbol**	**up**	**down**	**up**	**down**	
ILMN_1726448	MMP1		−4.3		−3.2	matrix metallopeptidase 1 (interstitial collagenase)
ILMN_1663873	MMP13		−2.9			matrix metallopeptidase 13 (collagenase 3)
ILMN_1778333	MMP24				−5.7	matrix metallopeptidase 24 (membrane-inserted)
ILMN_1796316	MMP9				−36.1	matrix metallopeptidase 9 (gelatinase B, 92kDa gelatinase, 92kDa type IV collagenase)
ILMN_1791796	MMP16		−2.0			matrix metalloproteinase 16 (membrane-inserted) transcript variant 2,
ILMN_1784459	MMP3		−2.3		−4.6	matrix metallopeptidase 3 (stromelysin 1, progelatinase) mRNA.

c: Matrix Metalloproteinases						
Years after treatment		**1&2**	**1&2**	**10**	**10**	
Gene ID	**Gene Symbol**	**up**	**down**	**up**	**down**	
ILMN_1702361	MMP16		−2.3		−8.1	matrix metallopeptidase 16 (membrane-inserted) (MMP16), transcript variant 2, mRNA.
ILMN_2399016	MMP28		−2.4			matrix metallopeptidase 28 (MMP28), transcript variant 3,
ILMN_1663873	MMP13		−2.9			matrix metallopeptidase 13 (collagenase 3)
ILMN_1685917	EMCN		−4.5			endomucin (EMCN),
ILMN_2160015	MMP21				−2.7	matrix metallopeptidase 21
ILMN_1736026	MMP8				−2.7	matrix metallopeptidase 8 (neutrophil collagenase)
ILMN_1718646	MMP15				−3.0	matrix metallopeptidase 15 (membrane-inserted)
ILMN_2073758	MMP12				−5.3	matrix metallopeptidase 12 (macrophage elastase)
ILMN_1786072	MEPE				−10.8	matrix extracellular phosphoglycoprotein

Table 2

Glycosaminoglycans

Years After Treatment		**1&2**	**1&2**	**10**	**10**	
Gene ID	**Gene Symbol**	**up**	**down**	**up**	**down**	
ILMN_1668760	HAS3	9.4				hyaluronan synthase 3 (HAS3), transcript variant 1,
ILMN_1794501	HAS3	4.2		2.8		hyaluronan synthase 3 (HAS3), transcript variant 1,
ILMN_1792978	HAS2	2.4		2.4		hyaluronan synthase 2 (HAS2),
ILMN_2243036	HAS2		−2.5			hyaluronan synthase 2 (HAS2),
ILMN_1754716	HAS1		−3.2		−47.3	hyaluronan synthase 1 (HAS1),
ILMN_1787548	HSPG2		−2.7			heparan sulfate proteoglycan 2 (HSPG2),
ILMN_1787548	HSPG2		−2.7			heparan sulfate proteoglycan 2 (HSPG2),
ILMN_2228035	HS3ST1	2.5				heparan sulfate (glucosamine) 3-O-sulfotransferase 1 (HS3ST1),
ILMN_1710416	HS3ST6			5.4		heparan sulfate (glucosamine) 3-O-sulfotransferase 6 (HS3ST6),
ILMN_1667432	HYAL3				−2.5	hyaluronoglucosaminidase 3 (HYAL3),
ILMN_2165463	HAPLN4				−2.7	hyaluronan and proteoglycan link protein 4 (HAPLN4),
ILMN_1712620	HYAL1				−4.2	hyaluronoglucosaminidase 1 (HYAL1), transcript variant 1,
ILMN_1740407	CHSY3			4.6		chondroitin sulfate synthase 3 (CHSY3),
ILMN_2165463	HAPLN4				−2.7	hyaluronan and proteoglycan link protein 4 (HAPLN4),
ILMN_2117845	CSPG4LYP2				−13.3	chondroitin sulfate proteoglycan 4-like, Y-linked pseudogene 2 (CSPG4LYP2), non-coding RNA.

Table 3

Fibronectin

Years after treatment		1&2	1&2	10	10	
Gene ID	Gene Symbol	up	down	up	down	
ILMN_2163873	FNDC1	5.0			−3.5	fibronectin type III domain containing 1 (FNDC1),
ILMN_1761084	FNDC5	3.9				fibronectin type III domain containing 5 (FNDC5)
ILMN_1675646	FN1			3.4		fibronectin 1 (FN1), transcript variant 7

Table 4

Micro array analysis of Laminin

Years after treatment		1&2	1&2	10	10	
Gene ID	Gene Symbol	up	down	up	down	
ILMN_1696434	LAMA1	2.0			−6.6	laminin, alpha 1 (LAMA1)
ILMN_2339266	LAMA2		−3.5			laminin, alpha 2 (LAMA2), transcript variant 1
ILMN_1653824	LAMC2		−2.2			laminin, gamma 2 (LAMC2), transcript variant 1
ILMN_1770038	LAMA1				−28.9	laminin, alpha 1 (LAMA1)
ILMN_2406035	LAMA3			10.7		laminin, alpha 3 (LAMA3), transcript variant 1
ILMN_1704247	LAMA3				−5.9	laminin, alpha 3 (LAMA3), transcript variant 2
ILMN_1800142	LAMB3			4.4		laminin, beta 3 (LAMB3), transcript variant 2
ILMN_1715684	LAMB3				−3.0	laminin, beta 3 (LAMB3), transcript variant 1
ILMN_1701424	LAMC2				−3.0	laminin, gamma 2 (LAMC2), transcript variant 1

Table 5

Proinflammatory genes

Years after treatment		1&2	1&2	10	10	
Gene ID	Gene Symbol	up	down	up	down	
ILMN_1704000	IL1F6	20.9				interleukin 1 family, member 6 (epsilon) (IL1F6),
ILMN_1765668	IL20RB	8.0			3.4	interleukin 20 receptor beta (IL20RB),
ILMN_1774874	IL1RN	5.6				interleukin 1 receptor antagonist (IL1RN), transcript variant 4,
ILMN_1798204	IL21R	5.4		16.4		interleukin 21 receptor (IL21R), transcript variant 2,
ILMN_2369221	IL15	4.7				interleukin 15 (IL15), transcript variant 1,
ILMN_1805385	IL22RA2	3.7				interleukin 22 receptor, alpha 2 (IL22RA2), transcript variant 1,

Years after treatment		1&2	1&2	10	10	
Gene ID	Gene Symbol	up	down	up	down	
ILMN_1758371	IL1R2	3.6				interleukin 1 receptor, type II (IL1R2), transcript variant 1,
ILMN_1658483	IL1A	3.6				interleukin 1, alpha (IL1A),
ILMN_2089875	TNFSF4	5.9				tumor necrosis factor (ligand) superfamily, member 4 (tax-transcriptionally activated glycoprotein 1, 34kDa) (TNFSF4),
ILMN_1699265	TNFRSF10B	2.5				tumor necrosis factor receptor superfamily, member 10b (TNFRSF10B), transcript variant 1,
ILMN_1655429	TNFAIP1	2.3		2.4		tumor necrosis factor, alpha-induced protein 1 (endothelial) (TNFAIP1),
ILMN_1784264	TNFSF13			9.7		tumor necrosis factor (ligand) superfamily, member 13 (TNFSF13), transcript variant gamma,
ILMN_2399190	TNFSF13			3.6		tumor necrosis factor (ligand) superfamily, member 13 (TNFSF13), transcript variant beta,
ILMN_2066858	TNFSF13B			2.5		tumor necrosis factor (ligand) superfamily, member 13b (TNFSF13B),
ILMN_1661343	TNFSF14				−2.3	tumor necrosis factor (ligand) superfamily, member 14 (TNFSF14), transcript variant 1,
ILMN_2106380	TNFSF15				−5.6	tumor necrosis factor (ligand) superfamily, member 15 (TNFSF15),
ILMN_2089875	TNFSF4			6.9		tumor necrosis factor (ligand) superfamily, member 4 (tax-transcriptionally activated glycoprotein 1, 34kDa) (TNFSF4),
ILMN_2048043	DEFB4	20.3				defensin, beta 4 (DEFB4),
ILMN_1705183	MPO	3.0				myeloperoxidase (MPO), nuclear gene encoding mitochondrial protein,

Table 6

Oxidative stress

Years after treatment		1&2	1&2	10	10	
Gene ID	Gene Symbol	up	down	up	down	
ILMN_1730054	GSTT1	48.1		51.7		glutathione S-transferase theta 1 (GSTT1),
ILMN_2321150	GSTTP2	4.6				glutathione S-transferase theta pseudogene 2 (GSTTP2), non-coding RNA. XM_941198 XM_945014 XM_945016
ILMN_2246548	GSTTP2				−4.2	glutathione S-transferase theta pseudogene 2 (GSTTP2), non-coding RNA. XM_941198 XM_945014 XM_945016
ILMN_1771964	GSTA4	3.3				glutathione S-transferase A4 (GSTA4),
ILMN_2218637	GSTM1L	2.9				glutathione S-transferase M1-like (GSTM1L), non-coding RNA.
ILMN_1789418	GSTT2	2.3				glutathione S-transferase theta 2 (GSTT2),

Years after treatment		1&2	1&2	10	10	
Gene ID	Gene Symbol	up	down	up	down	
ILMN_2246548	GSTTP2		−2.3			glutathione S-transferase theta pseudogene 2 (GSTTP2), non-coding RNA. XM_941198 XM_945014 XM_945016
ILMN_1716979	GSTM4		−2.9			glutathione S-transferase M4 (GSTM4), transcript variant 1,
ILMN_1691430	GSTCD			2.2		glutathione S-transferase, C-terminal domain containing (GSTCD), transcript variant 1,
ILMN_2168747	GSTA2			4.9		glutathione S-transferase A2 (GSTA2),
ILMN_1687387	MGST1			4.4		microsomal glutathione S-transferase 1 (MGST1), transcript variant 1d,
ILMN_1788122	GSTA5				−2.2	glutathione S-transferase A5 (GSTA5),
ILMN_2227817	GSTA3				−5.8	glutathione S-transferase A3 (GSTA3),
ILMN_1716979	GSTM4				−2.4	glutathione S-transferase M4 (GSTM4), transcript variant 1,
ILMN_1789418	GSTT2				−4.7	glutathione S-transferase theta 2 (GSTT2),
ILMN_1711642	GSTZ1				−8.8	glutathione transferase zeta 1 (maleylacetoacetate isomerase) (GSTZ1), transcript variant 3,
ILMN_1776214	TGM6				−10.3	transglutaminase 6 (TGM6),
ILMN_2193761	LOC442245		−3.0			glutathione S-transferase M1 pseudogene (LOC442245), non-coding RNA.
ILMN_1668134	GSTM1		−3.7			glutathione S-transferase M1 (GSTM1), transcript variant 1,
ILMN_1781952	MGST1		−3.6			microsomal glutathione S-transferase 1 (MGST1), transcript variant 1b,
ILMN_1786847	TGM3	6.0				transglutaminase 3 (E polypeptide, protein-glutamine-gamma-glutamyltransferase) (TGM3),
ILMN_2127416	GSR				−2.0	glutathione reductase (GSR),
ILMN_1811489	OXSR1	3.8		3.6		oxidative-stress responsive 1 (OXSR1),
ILMN_2319588	OSGIN1				−3.5	oxidative stress induced growth inhibitor 1 (OSGIN1), transcript variant 2,
ILMN_1686434	TXNDC6		−2.7			thioredoxin domain containing 6 (TXNDC6),
ILMN_1731137	TXNDC9	3.3				thioredoxin domain containing 9 (TXNDC9),
ILMN_1654457	TXN2			2.1		thioredoxin 2 (TXN2), nuclear gene encoding mitochondrial protein,
ILMN_2188155	TR2IT1		−2.1			thioredoxin reductase 2 intronic transcript 1 (TR2IT1),
ILMN_1799367	TXNDC14	4.5		4.4		thioredoxin domain containing 14 (TXNDC14),
ILMN_1717056	TXNRD1		−3.0			thioredoxin reductase 1 (TXNRD1), transcript variant 5,
ILMN_2258268	GLRX2				−13.1	glutaredoxin 2 (GLRX2), transcript variant 2,
ILMN_2222234	PRDX4	3.4				peroxiredoxin 4 (PRDX4),
ILMN_2395969	PRDX3		−2.1			peroxiredoxin 3 (PRDX3), nuclear gene encoding mitochondrial protein, transcript variant 1,

Years after treatment		1&2	1&2	10	10	
Gene ID	**Gene Symbol**	**up**	**down**	**up**	**down**	
ILMN_1775871	GPX5				−5.6	glutathione peroxidase 5 (epididymal androgen-related protein) (GPX5), transcript variant 1,
ILMN_2385410	GPX5				−10.4	glutathione peroxidase 5 (epididymal androgen-related protein) (GPX5), transcript variant 1,
ILMN_2133205	GPX2				−15.3	glutathione peroxidase 2 (gastrointestinal) (GPX2),
ILMN_1802706	IDH3G	7.3				isocitrate dehydrogenase 3 (NAD+) gamma (IDH3G), nuclear gene encoding mitochondrial protein, transcript variant 2,
ILMN_2363880	ALDH3B2	5.7				aldehyde dehydrogenase 3 family, member B2 (ALDH3B2), transcript variant 2,
ILMN_1677637	BDH1	5.0				3-hydroxybutyrate dehydrogenase, type 1 (BDH1), nuclear gene encoding mitochondrial protein, transcript variant 2,
ILMN_1679178	ATP5D	10.0				ATP synthase, H+ transporting, mitochondrial F1complex, delta subunit (ATP5D), nuclear gene encoding mitochondrial protein, transcript variant 1,
ILMN_1791754	CPT1B	10.0				carnitine palmitoyltransferase 1B (muscle) (CPT1B), nuclear gene encoding mitochondrial protein, transcript variant 3,
ILMN_1685703	ACOX2	8.5				acyl-Coenzyme A oxidase 2, branched chain (ACOX2),
ILMN_1654118	BCL2L1	8.1				BCL2-like 1 (BCL2L1), nuclear gene encoding mitochondrial protein, transcript variant 1,
ILMN_2198408	MFF	8.0				mitochondrial fission factor (MFF), nuclear gene encoding mitochondrial protein,
ILMN_2042343	MRPL42P5	6.1				mitochondrial ribosomal protein L42 pseudogene 5 (MRPL42P5), non-coding RNA.
ILMN_1700168	LARS2	4.1				leucyl-tRNA synthetase 2, mitochondrial (LARS2), nuclear gene encoding mitochondrial protein,
ILMN_1778187	TARS2	3.0				threonyl-tRNA synthetase 2, mitochondrial (putative) (TARS2), nuclear gene encoding mitochondrial protein,
ILMN_1733562	TFB1M	2.7				transcription factor B1, mitochondrial (TFB1M),
ILMN_1695472	MRPL10	2.6				mitochondrial ribosomal protein L10 (MRPL10), nuclear gene encoding mitochondrial protein, transcript variant 2,
ILMN_1727390	ATPAF2	2.5				ATP synthase mitochondrial F1 complex assembly factor 2 (ATPAF2), nuclear gene encoding mitochondrial protein,
ILMN_1752099	CYP11B2		−3.1			cytochrome P450, family 11, subfamily B, polypeptide 2 (CYP11B2), nuclear gene encoding mitochondrial protein,

Table 7

Apoptosis

Years after treatment		1&2	1&2	10	10	
Gene ID	Gene Symbol	up	down	up	down	
ILMN_2321720	CASP10	5.6		16.6		caspase 10, apoptosis-related cysteine peptidase (CASP10), transcript variant A,
ILMN_1683450	CDCA5	4.7				cell division cycle associated 5 (CDCA5),
ILMN_2192281	CARD8	4.1				caspase recruitment domain family, member 8 (CARD8),
ILMN_1787749	CASP8			5.1		caspase 8, apoptosis-related cysteine peptidase (CASP8), transcript variant C,
ILMN_1673757	CASP8			2.0		caspase 8, apoptosis-related cysteine peptidase (CASP8), transcript variant G,
ILMN_1722158	CASP5	3.4				caspase 5, apoptosis-related cysteine peptidase (CASP5),
ILMN_2326512	CASP1	3.0				caspase 1, apoptosis-related cysteine peptidase (interleukin 1, beta, convertase) (CASP1), transcript variant delta,
ILMN_2377733	CASP8	2.8				caspase 8, apoptosis-related cysteine peptidase (CASP8), transcript variant B,
ILMN_1739513	CASP14	2.7				caspase 14, apoptosis-related cysteine peptidase (CASP14),
ILMN_1678454	CASP4	2.4				caspase 4, apoptosis-related cysteine peptidase (CASP4), transcript variant alpha,
ILMN_1774585	CASP4			5.0		caspase 4, apoptosis-related cysteine peptidase (CASP4), transcript variant alpha,
ILMN_1778059	CASP4			2.1		caspase 4, apoptosis-related cysteine peptidase (CASP4), transcript variant gamma,
ILMN_1712532	CARD9	2.3				caspase recruitment domain family, member 9 (CARD9),
ILMN_1692349	CARD18	2.2				caspase recruitment domain family, member 18 (CARD18),
ILMN_2174437	CIDEC	2.2				cell death-inducing DFFA-like effector c (CIDEC),
ILMN_1666634	FAF1	2.0				Fas (TNFRSF6) associated factor 1 (FAF1),
ILMN_1736568	CASP2		−2.0			caspase 2, apoptosis-related cysteine peptidase (CASP2), transcript variant 3,
ILMN_1760227	CASP4		−2.1			caspase 4, apoptosis-related cysteine peptidase (CASP4), transcript variant delta,
ILMN_1667183	AIFM1		−2.3			apoptosis-inducing factor, mitochondrion-associated, 1 (AIFM1), nuclear gene encoding mitochondrial protein, transcript variant 2,
ILMN_2323172	CSF3R		−2.3			colony stimulating factor 3 receptor (granulocyte) (CSF3R), transcript variant 1,
ILMN_1747129	CASP8AP2		−3.3			CASP8 associated protein 2 (CASP8AP2),
ILMN_1659350	CASP6		−3.4			caspase 6, apoptosis-related cysteine peptidase (CASP6), transcript variant alpha,

Years after treatment		1&2	1&2	10	10	
Gene ID	**Gene Symbol**	**up**	**down**	**up**	**down**	
ILMN_2326509	CASP1		−3.5			caspase 1, apoptosis-related cysteine peptidase (interleukin 1, beta, convertase) (CASP1), transcript variant delta,
ILMN_1727762	CASP1			4.6		caspase 1, apoptosis-related cysteine peptidase (interleukin 1, beta, convertase) (CASP1), transcript variant alpha,
ILMN_2362974	CASP7				−3.4	caspase 7, apoptosis-related cysteine peptidase (CASP7), transcript variant delta,
ILMN_1730332	CASP7		−4.2			caspase 7, apoptosis-related cysteine peptidase (CASP7), transcript variant beta,
ILMN_1720360	BAD				−34.2	BCL2-antagonist of cell death (BAD), transcript variant 1,
ILMN_2384133	DFFB				−2.1	DNA fragmentation factor, 40kDa, beta polypeptide (caspase-activated DNase) (DFFB), transcript variant 3,
ILMN_1721978	CARD11			2.6		caspase recruitment domain family, member 11 (CARD11),
ILMN_1743714	CARD10			2.3		caspase recruitment domain family, member 10 (CARD10),
ILMN_2192281	CARD8				−2.1	caspase recruitment domain family, member 8 (CARD8),
ILMN_1671728	CARD14				−2.2	caspase recruitment domain family, member 14 (CARD14), transcript variant 1,
ILMN_1678962	DFFB				−6.9	DNA fragmentation factor, 40kDa, beta polypeptide (caspase-activated DNase) (DFFB),
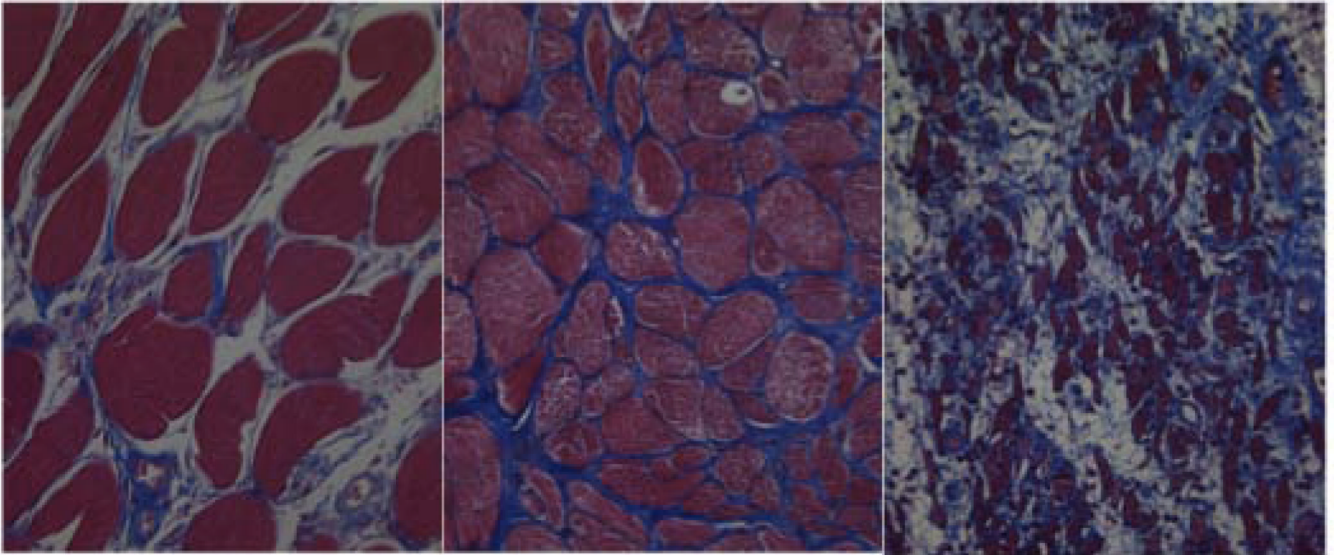
Figure 1.
Distorted muscle and collagen architecture in radiated specimens (a) Normal muscle and collagen architecture (b) Mild disorganization (c) Severe disorganization
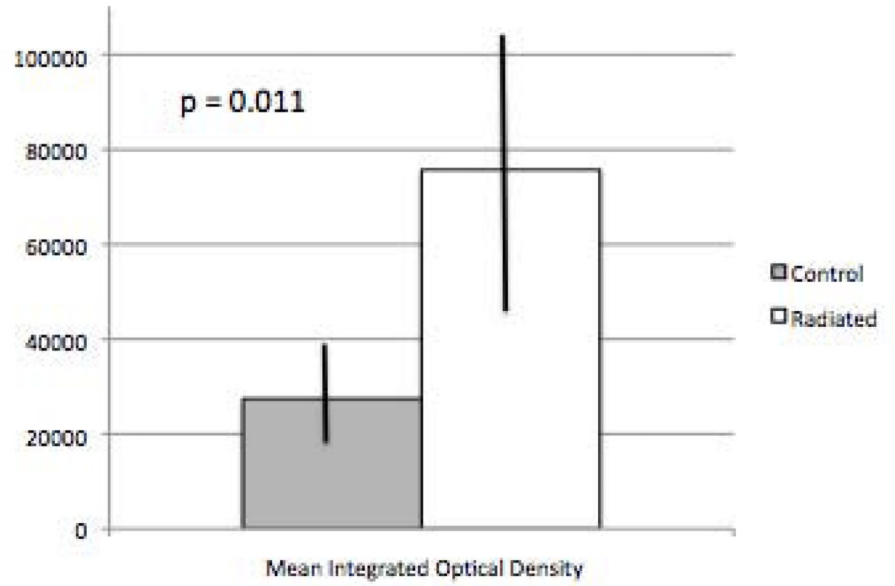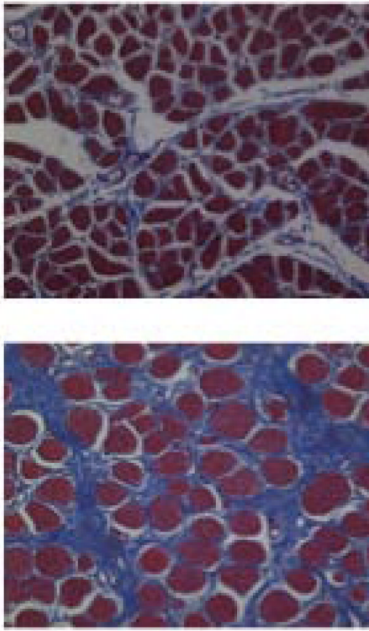
Figure 2.
Increased thyroarytenoid muscle collagen content in radiated specimens vs. controls (n = 12, p=0.011).
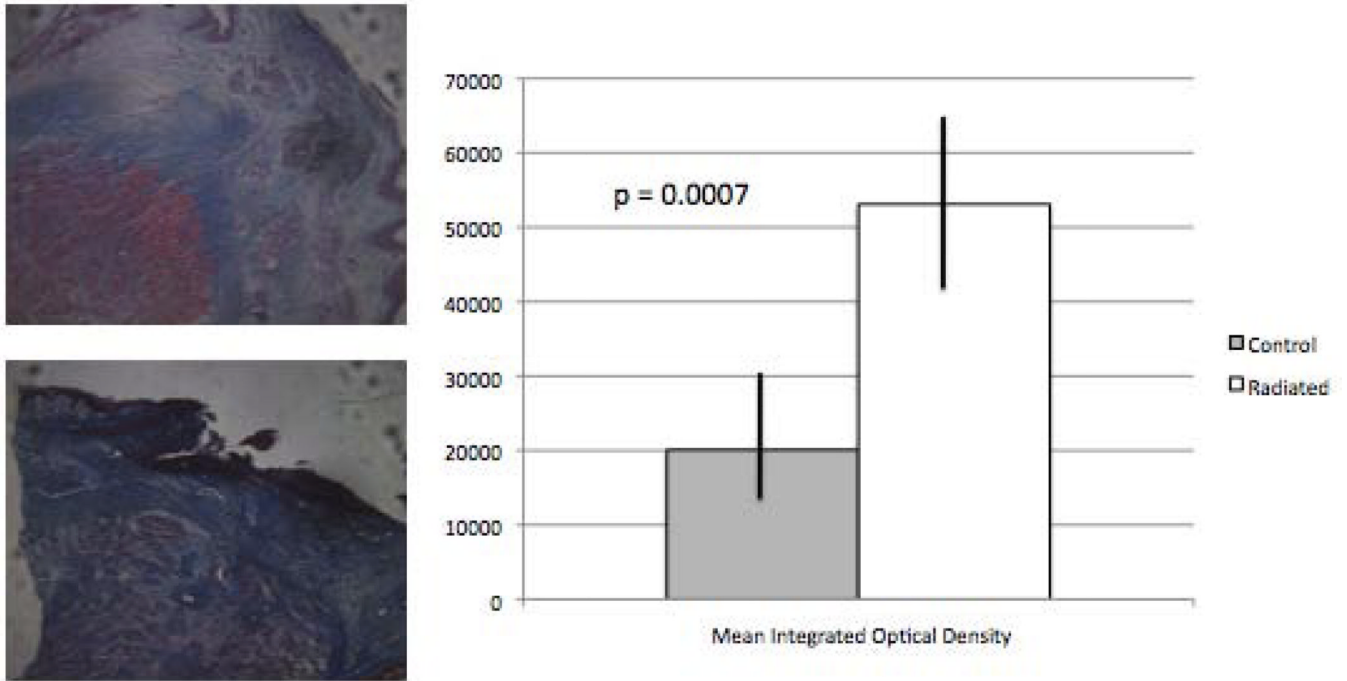
Figure 3.
Increased superficial lamina propria collagen content in radiated human vocal fold vs. controls (n = 13, p=0.0007).
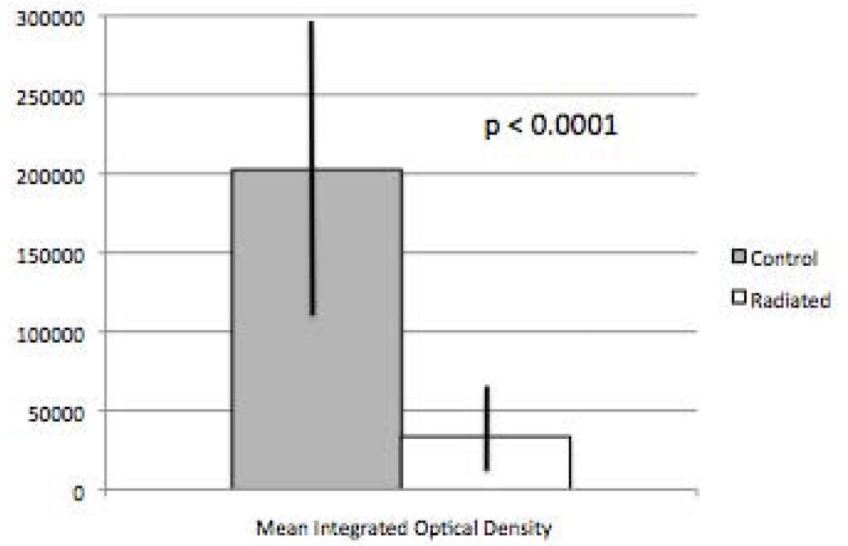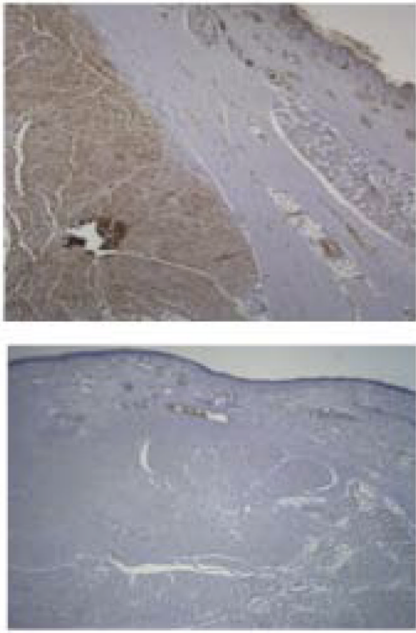
Figure 4.
Decreased thyroarytenoid muscle laminin content in radiated human vocal fold vs. controls
(n = 13, p<0.0001).
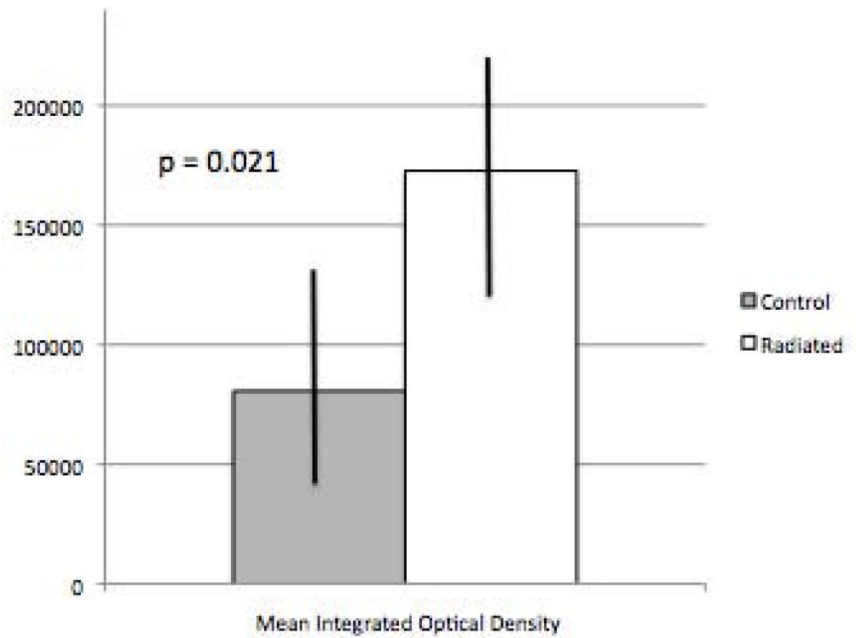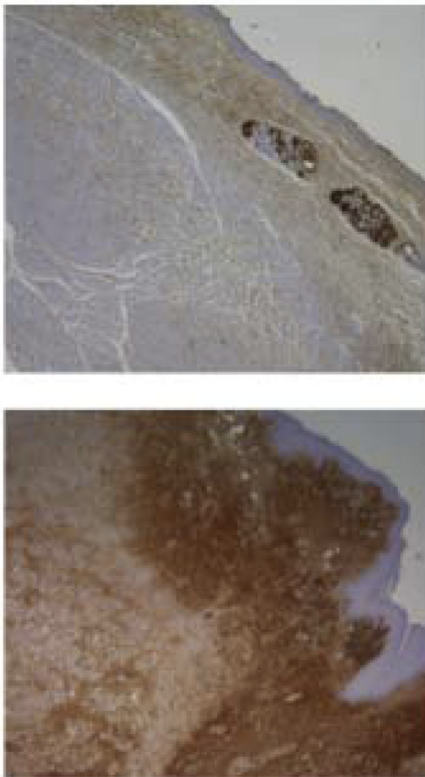
Figure 5.
Increased superficial lamina propria fibronectin content in radiated human vocal fold vs. controls (n = 12, p=0.021).
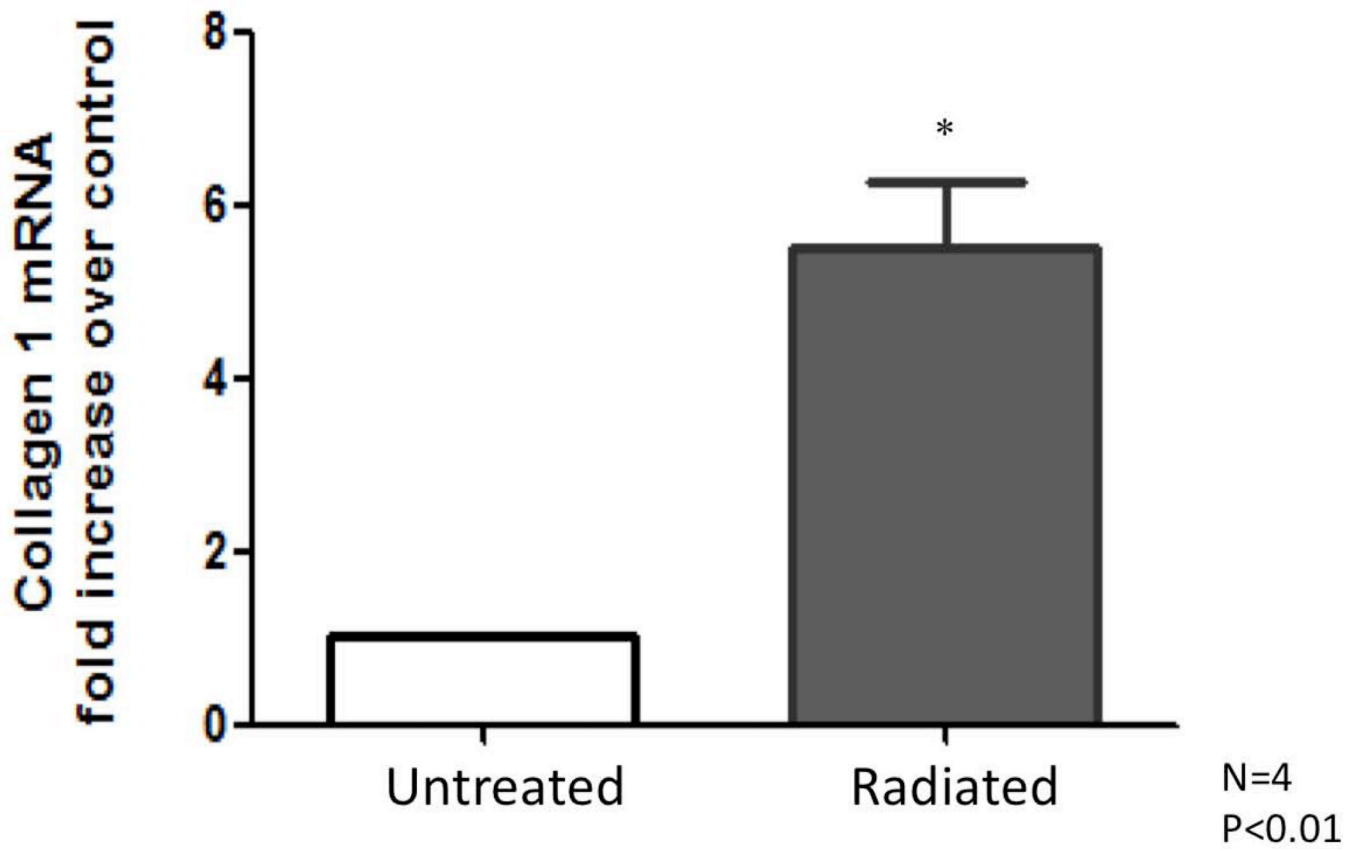
Figure 6.
Collagen 1 mRNA increases in radiated human vocal fold tissue compared to control
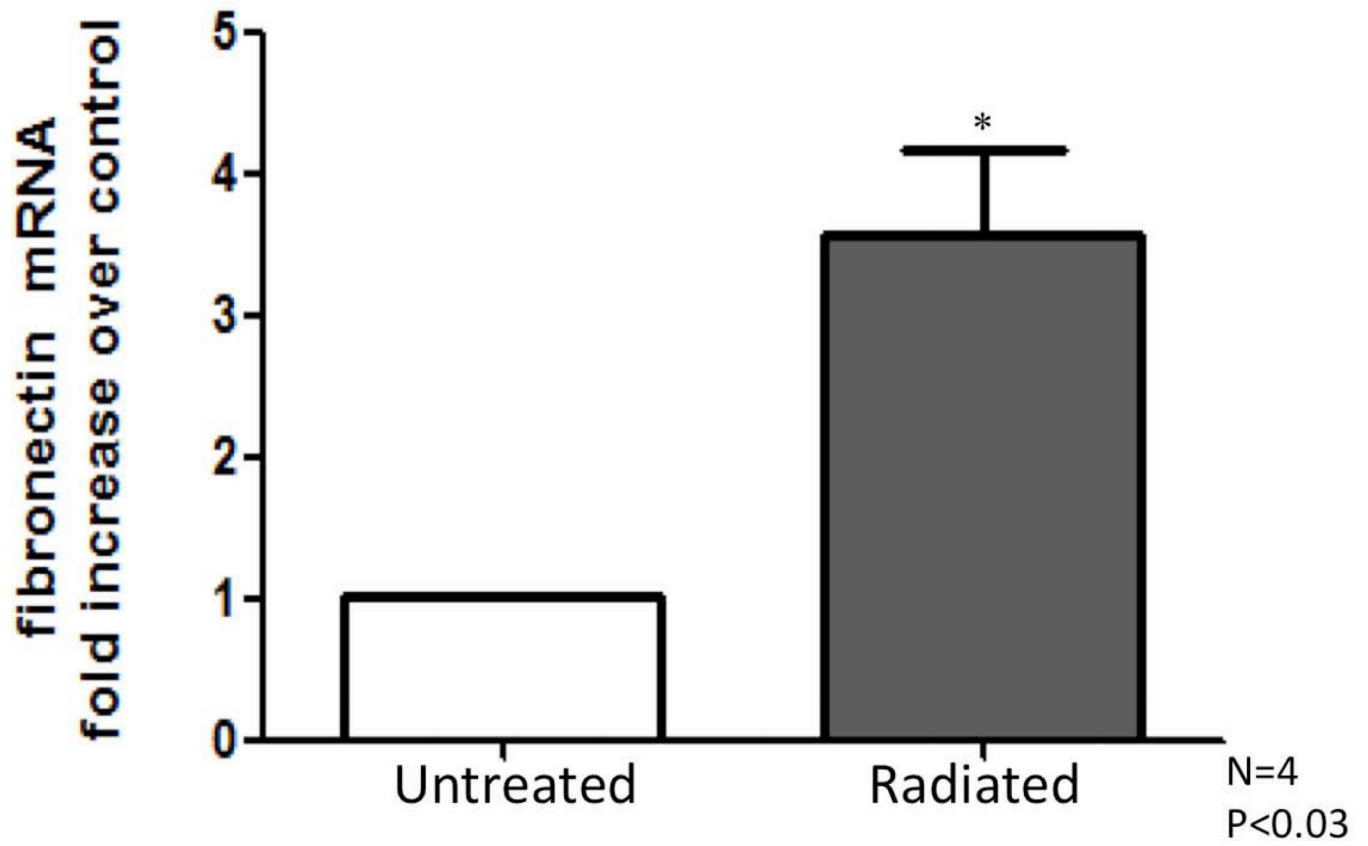
Figure 7.
Fibronectin mRNA increases in radiated human vocal fold tissue compared to control
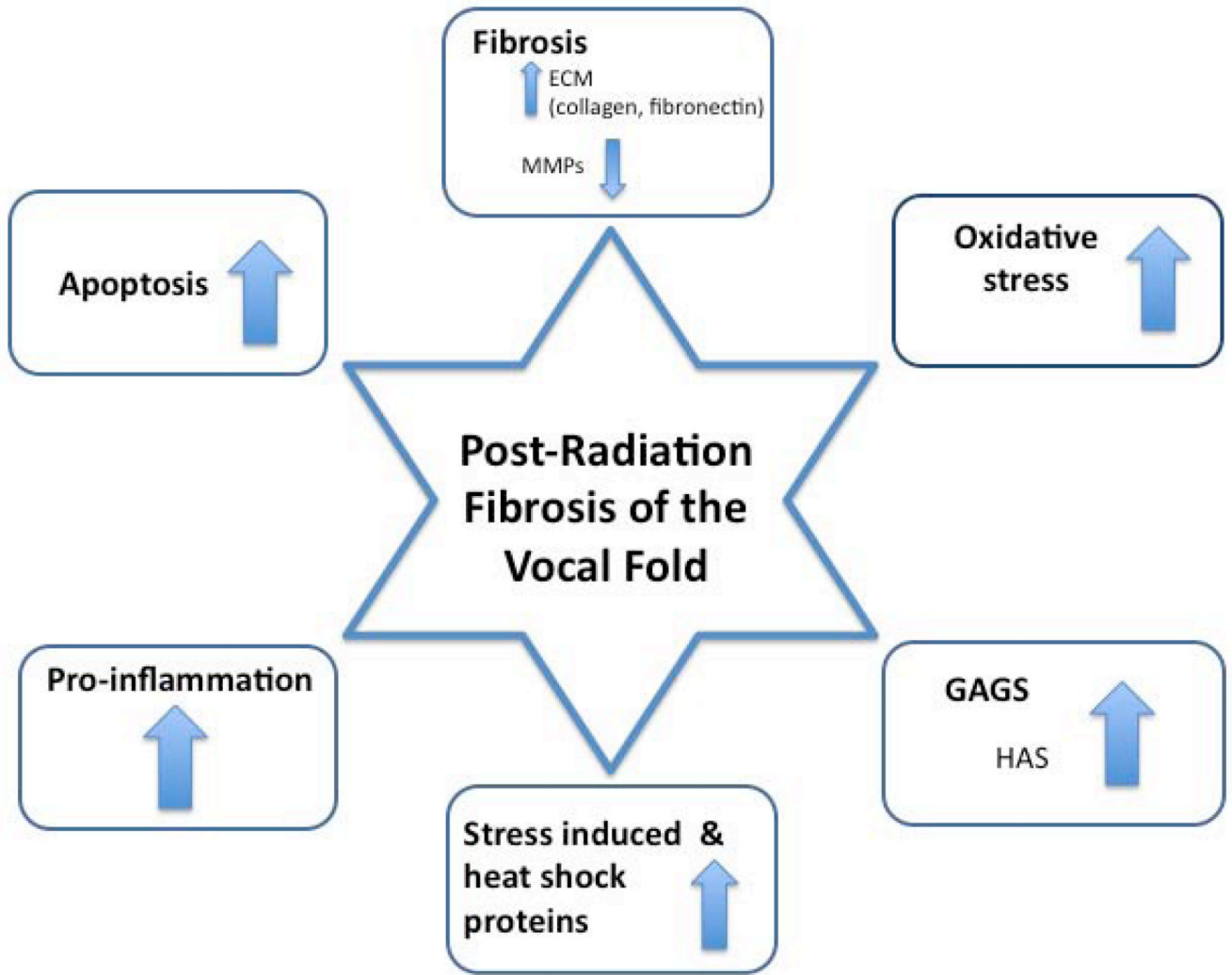
Figure 8.
Human Vocal Fold Radiation Fibrosis Summary
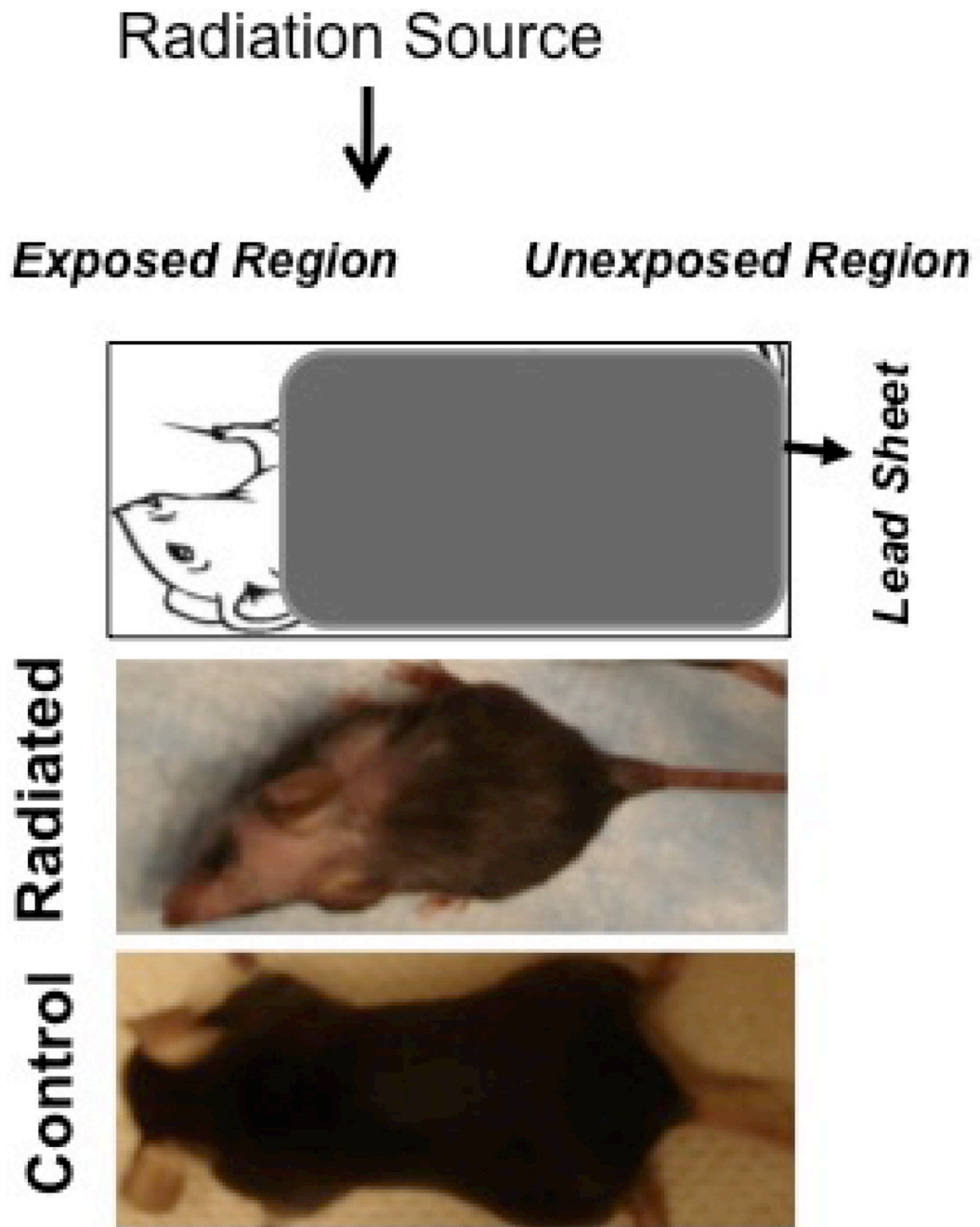
Figure 9.
Pigmentary change localized to cervical region after completion of radiation treatment.

A

Control
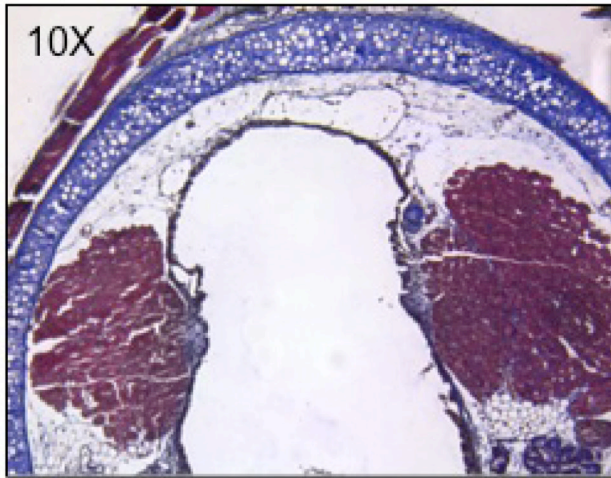
Radiated 5 gray 3 doses
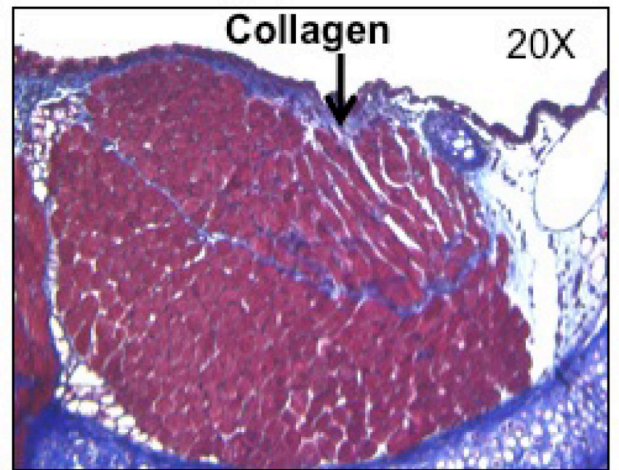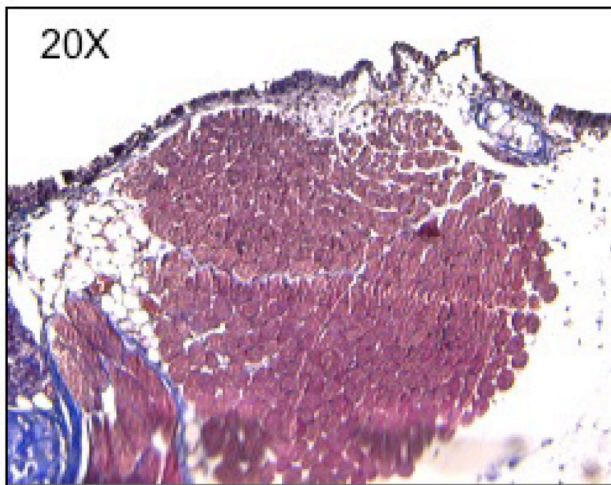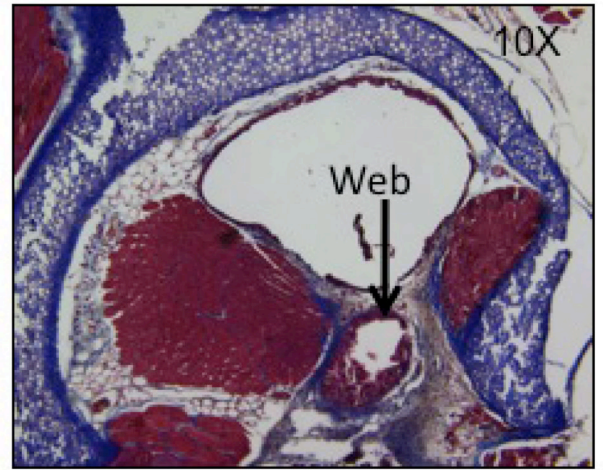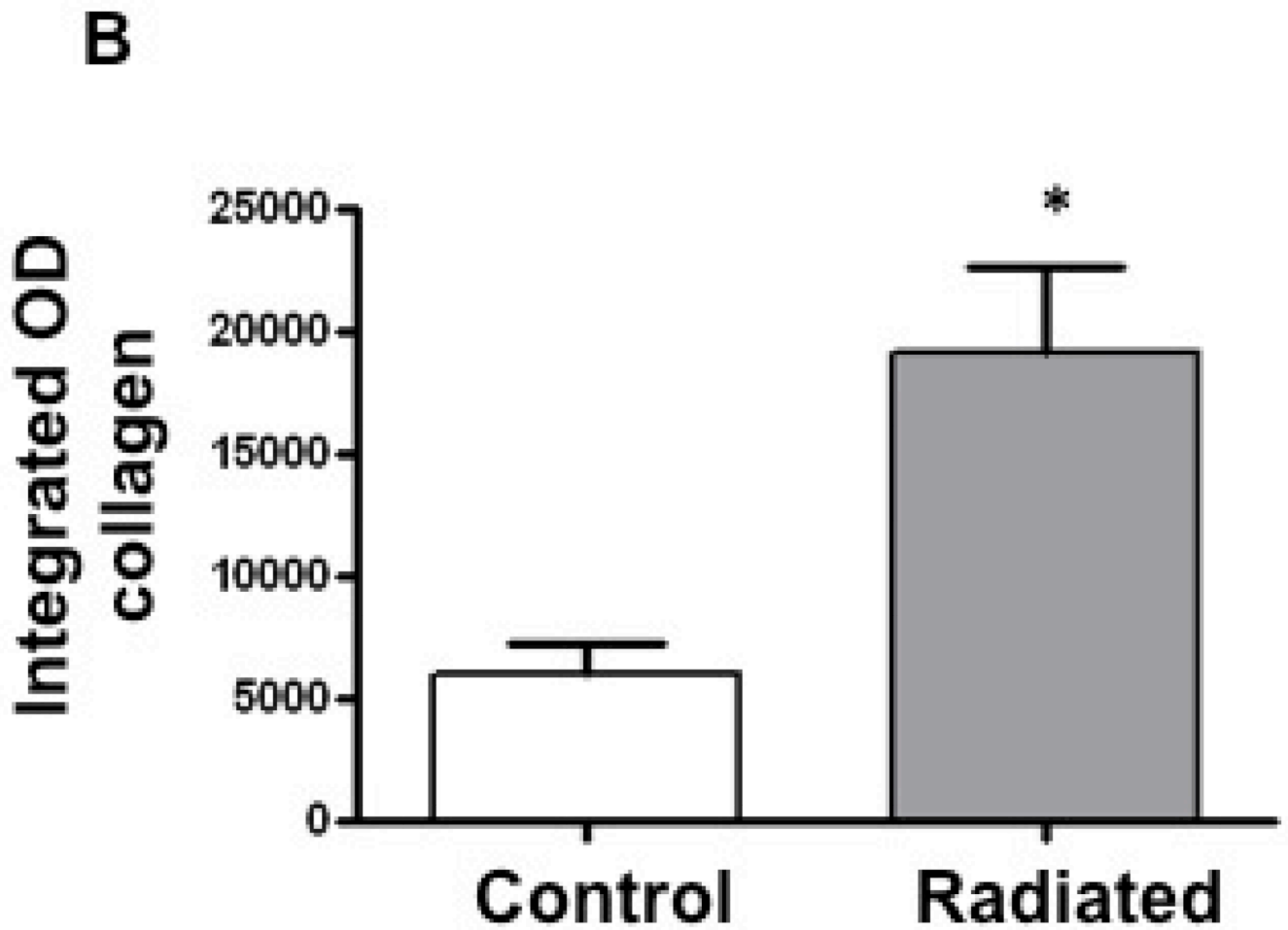
Figure 10.
Radiated mice demonstrated higher levels of Collagen deposition: a) Light microscopy
(20×) of vocal fold after Trichrome staining with increased collagen density staining blue. b)
Integrated optical density, representative of collagen content (n=8, p<0.002)

Control

Radiated 5 gray 3 doses

A

10X

Alcian blue Stain With Hyaluronidase

Alcian blue Stain With Hyaluronidase

10X

Alcian blue stain without Hyaluronidase

Alcian blue stain without Hyaluronidase
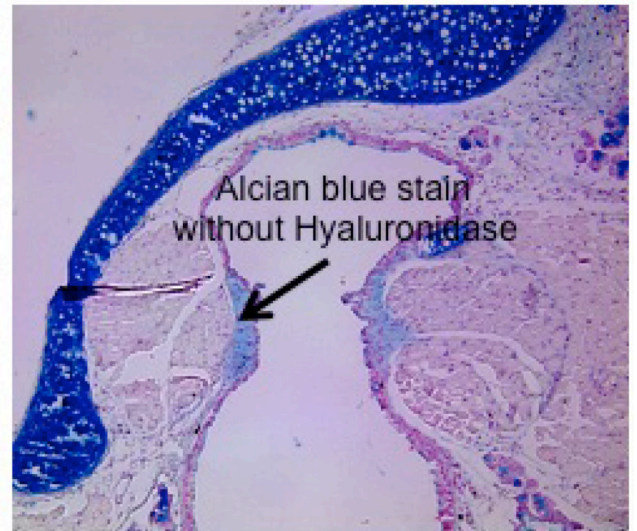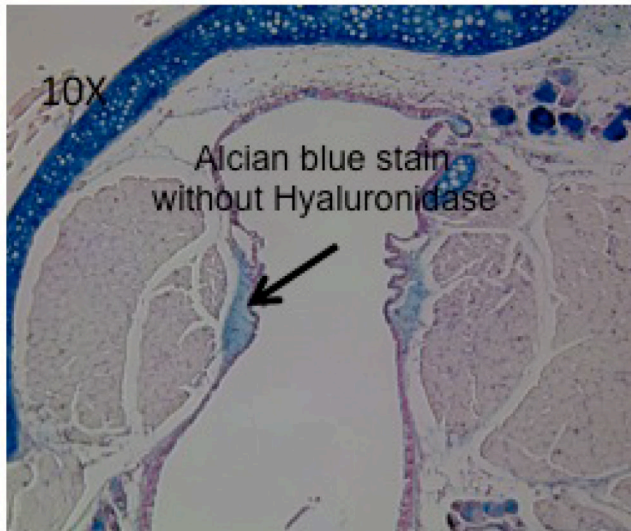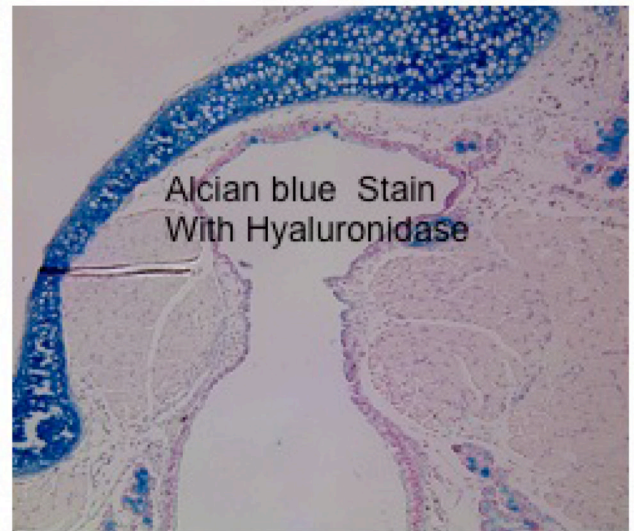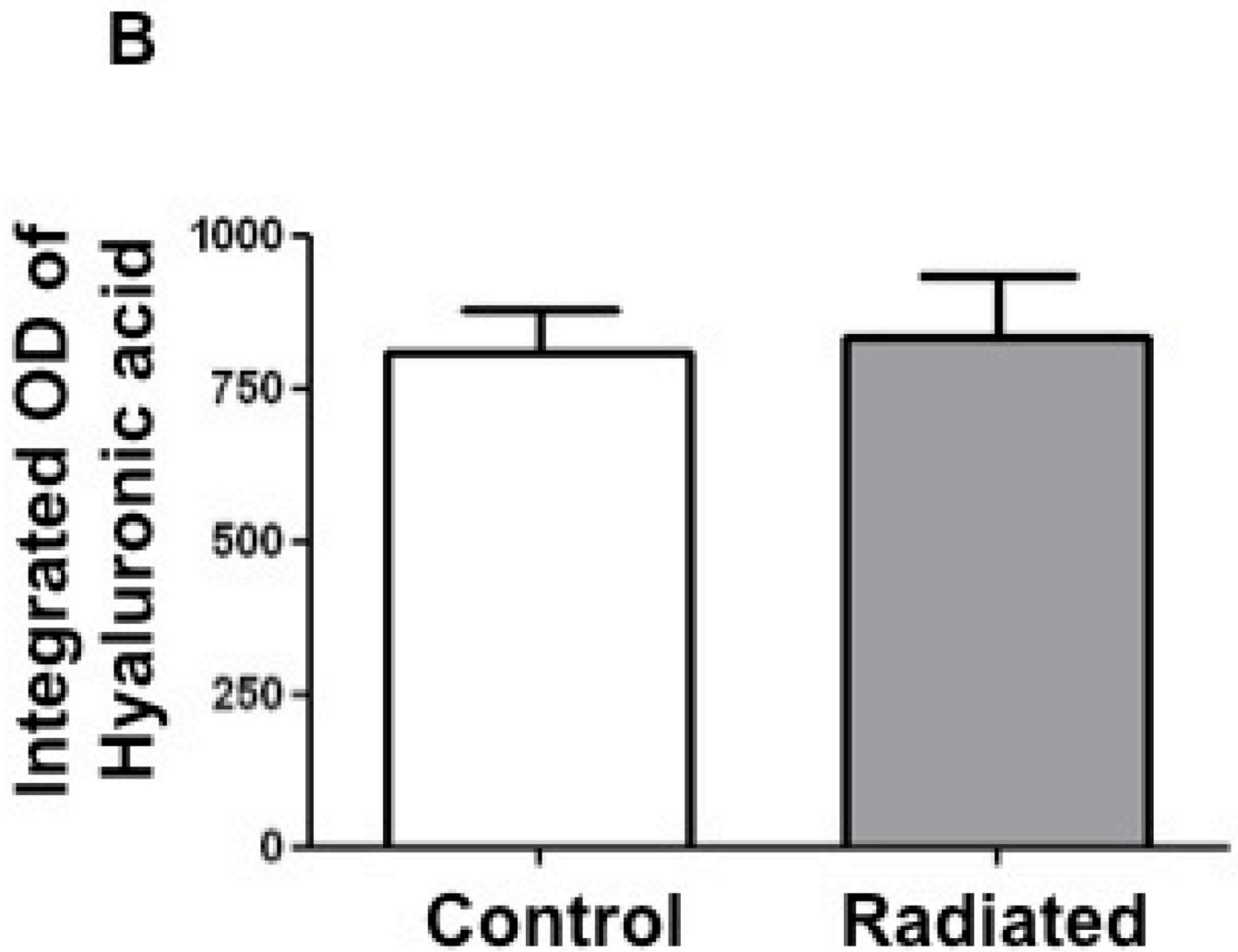
Figure 11.
Radiated mice larynges exhibit no change in hyaluronic acid (HA) levels compared to
control mice: a) Light microscopy (10×) of vocal fold after Alcian blue stain with hyaluronic
acid staining blue. b) Integrated optical density, representative of hyaluronic acid content
(n=8, p=0.82)

B
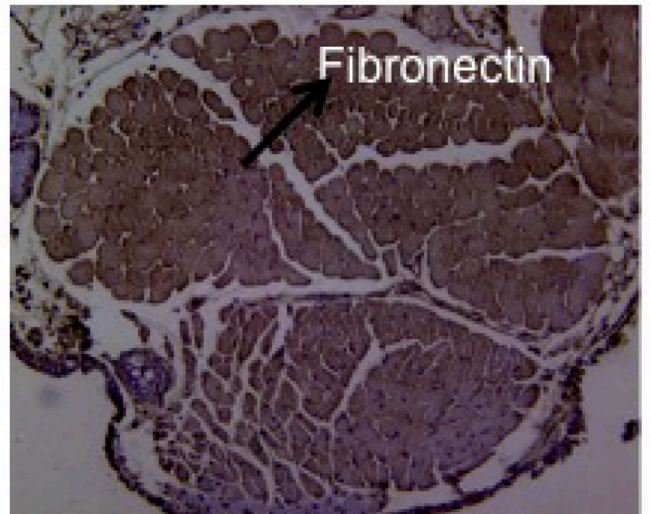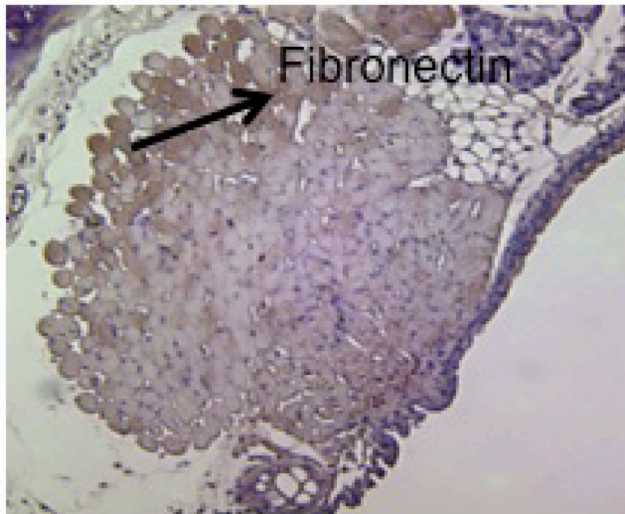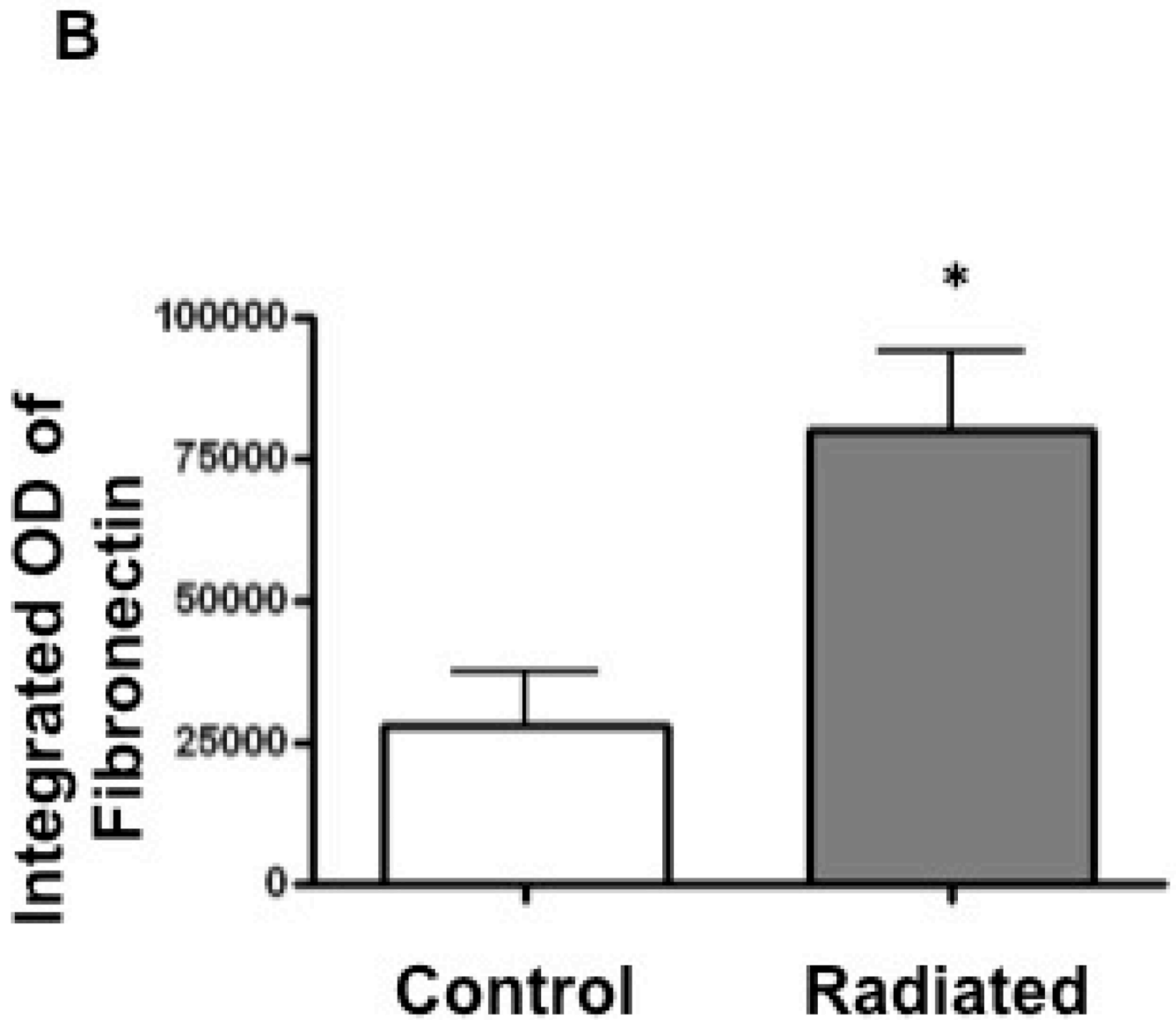
Figure 12.
Radiated murine vocal folds demonstrate increased fibronectin content with immunostaining: a) Light microscopy (10×) of vocal fold after fibronectin immunostain. b) Integrated optical density, representative of hyaluronic acid content (n=4, p<0.02)
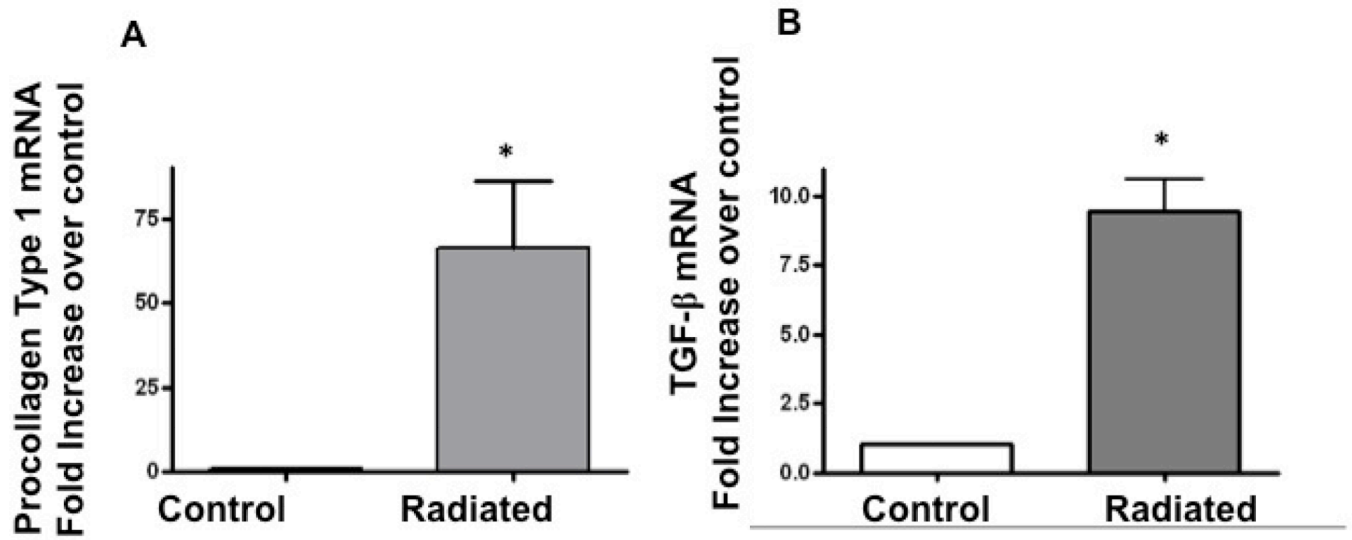
Figure 13.
Radiated mice demonstrate significantly higher levels of procollagen and TGF-β mRNA: a)
Increase in procollagen mRNA after radiation (n=5, p=0.048) b) Increase in TGF-β mRNA
after radiation (n=5, p=0.007)

Table 1

Historical and demographic data regarding radiated specimens

Mean age at time of surgery	59 years
Mean time interval from radiation completion to surgery	30 months (Range: 2 months – 10 years)
Gender	10 male, 3 female
Supraglottic primary	6
True glottic primary	3
Other	4